Novel ZnO nanoparticle activity against *Liberibacter crescens* growth and biofilm formation

by

Eber Naranjo

A thesis submitted to the Graduate Faculty of
Auburn University
in partial fulfillment of the
requirements for the Degree of Master of Science

Auburn, Alabama
August 4, 2018

Keywords: *Liberibacter, biofilm, planktonic, ZnO, nanoparticle, Zinkicide*^{TM}.

Approved by

Leonardo De La Fuente, Chair, Associate Professor of Plant Pathology
Mark Liles, Professor of Biological Sciences
Joseph Kloepper, Professor of Plant Pathology
Paul Cobine, Associate Professor of Biological Sciences

Abstract

Huanglongbing (HLB) or citrus greening is the most devastating citrus disease worldwide and it severely affects the US citrus industry with millionaire losses annually. The phloem limited, insect vectored and uncultivable nature of its causal agent, '*Candidatus* Liberibacter asiaticus', makes this disease to be incurable and unmanageable to the date by conventional methods. In this work, the in vitro antimicrobial activity of Zinkicide™, a novel ZnO based nano-formulation, was evaluated in batch cultures and under flow conditions, using *Liberibacter crescens* (Lcr) as a biological model for *Liberibacter* spp.

Initially, cultural factors to obtain Lcr in biofilms in vitro were studied. Media optimization was performed by manipulating concentrations of methyl-β-cyclodextrin (mβc) and fetal bovine serum (FBS) in media BM7. The use of the alamarBlue® cell proliferation kit confirmed mβc stimulates Lcr viability and showed Lcr forms more biofilm in response to adverse environments. Cell adhesion force assays in microfluidic chambers (MC) and biofilm quantification in batch cultures confirmed that the BSA contained in the FBS fraction of the BM7 medium, prevents cell-surface attachment and demonstrated that Lcr-surface attachment does not rely on protein synthesis. Cell-cell aggregation assays showed Lcr aggregates more in the optimized media formulation than in BM7. Microscopic characterization of floating and attached Lcr biofilms showed both structures are embedded in an EPS extracellular matrix and that surface-attached biofilms are formed mainly on the flask bottom. Optimum conditions to assess Lcr growth and cell viability in microfluidic chamber systems were also determined.

Zinkicide™ minimum inhibitory concentration in microtiter assays was 52ppm, while the minimum bactericidal concentration was 183ppm. When used at 104ppm, the compound inhibited more than the 96% of the biofilm formation. Zinkicide™ was not effective disrupting preformed biofilms in 96 well plates. In MC, Zinkicide™ did not disrupt initially Lcr adherent cells or disrupted preformed biofilms, but the occurrence of massive cell membrane damage on the Zinkicide™ treated main channels for both experiments was revealed by using the DEAD/LIVE Bactlight viability kit. The spatial antimicrobial activity assessment of Zinkicide™ in MC, showed this compound acts in gradients in fluidic vessels according to structural splits, flow direction, and cell concentration.

In summary, in this work we described by the first time the biofilm formation process for the *Liberibacter* genus, and identified the cultural factors that trigger this phenome in vitro. We also evaluated the capacity of Zinkicide™ to inhibit Lcr growth and biofilm formation and discovered an unexpected resilience of Lcr biofilms against this antimicrobial compound.

Acknowledgments

I would like to thank to my lab members and visitors Prem Kandel, Honyu Chen, Hajeewaka Mendis, Marcus Silva, Edel Pérez, Qing Ge, Luca De Vicentti, Giussy D´ Atoma for their comments in order to improve this work during our lab meetings.

Special thanks to Laura Melisa Gomez and Sy Traore for being my closest friends during this process and to Virginia Ferreira for being a great research partner and for spending hours struggling at my side to obtain those great confocal microscopy images.

I thank to my committee members, Dr Koeppler, Dr Mark Liles and Dr. Paul Cobine for their comments and suggestions for the development of the project.

I specially thank to my advisor, Dr. Leonardo De La Fuente, for his positive energy and patience, for the freedom he gave me for developing my new ideas, his encouragement for independence development and time management, and above all, for putting me back on track in research.

I am deeply grateful to people who trusted on me and showed their support in the hardest moments. To my Spanish brother Javier Peñalver, to my former advisor and role model, Dr. Maria Milagros Lopez. To people that became my family, Katherine Espinoza, Sara Morales and Marisol Espinoza. Nothing of this would be possible without their presence.

I thanks to Dr. Gabriela Chavez, for potentiating my skills, for bringing balance to my days, for her patience and for her unconditional love and support.

Finally, I would like to thank to my parents and siblings, they are the first responsible for everything I can accomplish in my life.

Table of Contents

Abstract ii

Acknowledgments iv

List of Tables vii

List of Illustrations viii

List of Abbreviations ix

Chapter 1: A literature review linking *Liberibacter* spp., biofilms and ZnO nanoparticles 1

The *Liberibacter* genus 1

Plant diseases caused by *Liberibacter* spp. 1

General life cycle of pathogenic *Liberibacter* spp 4

Biofilm formation as an important step in *Liberibacter* spp. life cycle 5

Liberibacter crescens: A culturable proxy to study unculturable *Liberibacter* spp. 5

HLB: The most serious disease caused by *Liberibacter* spp. in the US 6

HLB Symptomatology 7

Economic impact of HLB in the US 8

HLB disease Management 8

Zinc oxide nanoparticles as antimicrobial compounds 10

Zinkicide^{TM} as a chemical control candidate for HLB 11

Overall hypothesis 12

Main objective 12

Specific objectives 13

References 13

Chapter 2: *Liberibacter crescens*, the only culturable member of its genus, forms biofilm under specific culture conditions 18

Abstract 19

Introduction 20

Materials and Methods 23

Results 30

Discussion 42

References 49

Chapter 3: In vitro antimicrobial activity of a zinc-based nanoparticle compound, Zinkicide™, against *Liberibacter crescens*, as a biological model for pathogenic *Liberibacter* spp. 53

Abstract 54

Introduction 57

Materials and Methods 59

Results 62

Discussion 71

References 77

List of Tables

Table 1-1. Characteristics of *Liberibacter* spp. 2

Table 2-1. Formulation for 1L of the main media used in this work ..... .24

Table 2-2. Pearson r coefficient values for the linear regression analysis between each culture fraction quantified at 6dpi and FBS concentration values……..... .34

Table 2-3. Table 2-3. Pearson r coefficient values for the linear regression analysis between each culture fraction quantified at 6dpi and mβc concentration values from 0 to 0.75g/l. 34

Table 2-4. Pearson r coefficient values for the linear regression analysis between each culture fraction quantified at 6dpi and the alamarBlue® percentage reduction (ABPR) for mβc concentration value from 0 to 0.75g/l. 36

Table 3-1. Colony forming units per ml (CFU/ml) recovered in BM7 agar plates for each Zinkicide™ concentration value tested in the MBC concentration range. 63

List of Illustrations

Figure 2-1. Lcr growth in FBS concentration gradients..... 32

Figure 2-2. Lcr growth in mβc concentration gradients..... 33

Figure 2-3. Lcr cell viability and culture fraction ratios variation in response to different mβc concentrations.....35

Figure 2-4. Lcr attachment force assessment in MC……..... .37

Figure 2-5. Characterization of GFP-Lcr floating biofilms in batch cultures by CLSM at 7dpi……..... 38

Figure 2-6. Three-dimensional characterization of Lcr attached biofilms by CLSM. 40

Figure 2-7. Microscopic characterization of Lcr biofilms in MC……..... 41

Figure 3-1. Lcr total growth inhibition from 26 to 104ppm of Zinkicide™ in BM7 medium…….....……..... 63

Figure 3-2. Biofilm formation inhibition activity of Zinkicide™ against Lcr 64

Figure 3-3. Zinkicide™ effect on Lcr preformed biofilms 8 days after application.…..... 65

Figure 3-4. Biofilm formation inhibition and biofilm disruption assays in microfluidic chambers. …….....67

Figure 3-5. Spatial antibacterial activity of Zinkicide™, against Lcr in microfluidic chambers (MC) assessed by the LIVE/DEAD® BactLight Bacterial viability kit …..... 68

Figure 3-6. *L. crescens* ROS formation in response to Zinkicide™. 73

List of Abbreviations

HLB	Huanglongbing
CLas	'*Candidatus* Liberibacter asiaticus'
CLso	'*Candidatus* Liberibacter solanacearum'
Lcr	*Liberibacter crescens*
FBS	fetal bovine serum
mβc	Methyl-β-cyclodextrin
ABPR	alamarBlue® percentage reduction
MC	microfluidics chambers
BSA	Bovine serum albumin
EPS	Exopolysaccharide
ZnO	Zinc oxide
Np	nanoparticle
MIC	minimum inhibitory concentration
MBC	minimum bactericidal concentration

Chapter 1: A literature review linking *Liberibacter* spp., biofilms and ZnO nanoparticles.

The *Liberibacter* genus

The *Liberibacter* genus is comprised by non-motile gram-negative bacterial rods that are phloem limited inside their plant hosts and vectored by insects (1). Phylogenetic analysis suggest the *Liberibacter* genus evolved from the Rhizobiaceae family through reductive evolutionary processes that occurred during host adaptation (2). As a result of living on this close dependence of their hosts, these species exhibit a reduced genome of 1.5 Mb or less, display a DNA G+C content of 31–37 %, similar to many insect symbionts, and in most of cases are yet unculturable in vitro (2, 3). Some of the *Liberibacter* spp. characteristics as well as the diseases associated to these species are shown in Table 1-1.

Plant diseases caused by *Liberibacter* spp.

Liberibacter spp. are causal agents of old and newly emergent plant diseases (2). HLB or Citrus greening is caused by '*Candidatus* Liberibacter asiaticus' (CLas) and '*Candidatus* Liberibacter americanus' (CLam), which are transmitted by the Asian citrus psyllid (ACP) *Diaphorina citri* and a third species, '*Candidatus* Liberibacter africanus' (CLaf) that is transmitted by the African citrus psyllid *Trioza erytreae* (2). HLB is a centenary citrus disease, that was first reported under several names in different Asian locations in the 19th an early 21st centuries (4). The insect-vectored nature of this disease was noticed early (4), but its bacterial etiology was not confirmed until 1984, when Garnier et al. demonstrated the presence of peptidoglycan on the membrane of these microorganisms (5). Nowadays, HLB is still as a major problem in the places where it was first described (6) and represent the most serious threat to the citrus industry worldwide (4).

Table 1-1. Characteristics of *Liberibacter* spp.

Species	Plant hosts	Insect vector	Disease	Geographic distribution	Genome size (Mpb)	References
Candidatus Liberibacter asiaticus (CLas)	Rutaceae	Asian citrus psyllid (*Diaphorina citri*)	HLB	Asia, Africa, Oceania and the Americas	1.23	(2, 7–10)
Candidatus Liberibacter americanus (CLam)	Rutaceae	Asian citrus psyllid (*Diaphorina citri*)	HLB	Brazil	1.17	(3, 9, 11)
Candidatus Liberibacter africanus (CLaf)	Rutaceae and Apocynaceae	*African citrus psyllid (Trioza erytreae)*	HLB	Africa	1.19	(3, 9, 12, 13)
Candidatus Liberibacter solanacearum (CLso)	Solanaceous and Apiaceous crops	*Tomato/potato psyllid (Bactericera* spp.), *Trioza apicalis*	Zebra chip in potato, Vegetative disorders	Central and North America, Europe	1.26	(3, 9, 14)
Candidatus Liberibacter europaeus (CLeu)	Rosaceae plants	*Arytainilla spartiophila*	Endophyte	Italy, Hungary	unknown	(3, 15)
Liberibacter crescens (Lcr),	*Carica stipulata×C. pubescens,* *Citrus japonica, Bergera koenigii*	Unknown	Papaya bunchy top (PBT) HLB-like symptoms	Puerto Rico, United States	1.5	(9, 16)

The second most relevant disease caused by *Liberibacter* spp. in agriculture, is a vascular disorder in potato named Zebra chip (ZC). Zebra chip has been described associated with CLso (3, 17, 18). This bacterium was first described by Hansen et al. (18) and Liefting et al. (17) in New Zealand and the US respectively, associated with a debilitating yellowing plant condition in tomato and potato called "psyllid yellows". Since its first detection, CLso has been reported associated with vegetative disorders in pepper (19), tobacco (20), carrot (21), celery (22), bittersweet (23), Silverleaf Nightshade (*Solanum elaeagnifolium*) (24), and more recently in chervil, fennel, parsley, and parsnip (25). This pathogen is especially harmful in the potato industry where it can reduce yields in ~60% (17) and decreases the marketable value of remaining tubers by the antiesthetic discoloration pattern observed in the potato chips after frying (26). In 2009 this disease was prevalent in most potato-producing states in the US, and reached epidemic levels in 2011 in the Pacific Northwest states (27).

Another *Liberibacter* species, '*Candidatus* Liberibacter europaeus' was described in New Zealand, causing symptoms of stunted growth of shoots, shortened internodes, leaf dwarfing and leaf tip chlorosis in *Cytisus scoparius*, an invasive leguminous exotic shrub (15). This bacterium was later detected in high titers in multiple Rosaceae plants, including apple, blackthorn, hawthorn, and pear, however, the absence of symptoms in these cultivars attributed and endophytic behavior for this species (3).

Liberibacter crescens¸ the only culturable species of the genus, was found in high titers in the phloem sap of a mountain papaya plant (*Carica stipulata*×*C. pubescens*) in Puerto Rico, showing symptoms of a disease known as papaya bunchy top (PBT) (1). The lack of fulfilment

of Koch's postulates for this species led to the initial classification of Lcr as an endophyte (9). However, a recent report based in the multilocus sequence analysis of four housekeeping genes, identified a new '*Candidatus* Liberibacter crescens' associated with HLB-like symptoms in plants of the Rutaceae family, including kumquat (*Citrus japonica*) and curry (*Bergera koenigii*) in the US (16). Even though no Koch's postulates have been fulfilled for this possibly emergent species, it is opening questions about Lcr pathogenicity and adds relevance to the only cultivable species of the genus.

General life cycle of pathogenic *Liberibacter* spp.

This section will describe a general life cycle common for CLas and CLso because of their major impact in worldwide agriculture. Both CLas and CLso multiply in the plant and their psyllid host (28). Once a healthy plant is infected, there is a latency period that last between 6 and 12 months for HLB (29) and from 21 to 28 days for ZC (30), in which no evident symptoms are observed but the plant may act as a source of the bacterium. During this time, *Liberibacter* spp. move systemically following the translocation of the phloem sap, and accumulates and multiplies in the sieve tubes of sink organs such as young leaves, seed coat, and roots (3). *Liberibacter* spp. are then acquired by their vectors during their feeding from the phloem of infected plants, specially from fresh flushes, and in some cases may immediately be transmitted into healthy host plants (31). In other cases, around a two weeks latency period is necessary before the psyllids are able to transmit the bacterium (32, 33). Inside their insect vectors, *Liberibacter* spp. extensively multiplies and colonize salivary glands, hemolymph, filter chamber, midgut, fat and muscle tissues, and ovaries (34), reaching up to 10^4 genome copies per psyllid for CLso (35), and up to 10^7 bacteria per insect for CLas (36). After reaching a threshold level of infective bacteria, any

psyllid can then spread the pathogen during their phloem feeding to surrounding healthy plants in a stochastic manner (36).

Biofilm formation as an important step in *Liberibacter* spp. life cycle

Microscopic analyses in planta show that CLas and CLso cells growth planktonically in the plant phloem sap without attaching to the sieve tube cell walls or forming cell-cell aggregates (3). Same growth mode is displayed in the insect hemolymph, where *Liberibacter* spp. cells growth dispersed and individually (31). However, studies based in fluorescent in-situ hybridization techniques, demonstrate that *Liberibacter* spp. form extensive biofilms in cells of the salivary glands, midgut and salivary psyllid organs (37–39). These results were supported by the comparison of healthy and infected African and Asian citrus psyllids gene expression profiles, that showed an overexpression of bacterial genes involved in motility, cell-surface attachment and biofilm formation (28, 40). Overall scientific evidence suggests biofilm formation plays an important role during *Liberibacter* spp. psyllid life stage, whether by providing an adaptable status for efficient insect transmission, or by offering shelter from the insect immune system or unfavorable conditions (2, 37). Therefore, the study of the biofilm formation process of *Liberibacter* spp. may disclose new mechanisms involved in the transmission and persistence of these organisms in their insect vectors and may provide targetable spots in the life cycle of these harmful pathogens.

***Liberibacter crescens*: A culturable proxy to study unculturable *Liberibacter* spp.**

Comparative genomics analysis between Lcr, CLas and CLso revealed the presence of several genes involved in the synthesis of aromatic amino acids, several vitamins, histidine, cysteine,

lipopolysaccharides, and fatty acids in Lcr, that are absent in the unculturable species (41). These previous findings may explain why this species can be grown in pure culture in vitro despite its still fastidious nature (9). *Liberibacter crescens* displays an average nucleotide identity (ANI) of 77 and 78% with CLas and CLso respectively, and as its near unculturable relatives, it was described as a phloem-limited bacterium. The close phylogenetic relationship of Lcr with unculturable *Liberibacter* spp., its common habitat origin, and its capacity to growth in pure culture in vitro, makes of this species the best biological model to predict unculturable *Liberibacter* spp. behavior in vitro. As a result, Lcr has been used as a valuable tool for studies in *Liberibacter* spp. comparative genomics (1, 14, 41, 42), heterologous expression of CLas genes (43–45) and was used in this work as a surrogate for unculturable *Liberibacter* spp.

HLB: The most serious disease caused by *Liberibacter* spp. in the US

In the US, HLB is caused by the pathogenic system of CLas and the ACP *Diaphorina citri*. *Diaphorina citri* was first detected in the US in 1998 limited to dooryard host plantings on the east coast of Florida; by September 2000, the insect was already spread to 31 Florida counties (46). Five years later, in 2005, HLB was reported by the first time in the US, in South Miami-Dade county, and 3 years later, a Federal order was issued to quarantine the entire state of Florida (47). At the present time, HLB is prevalent in the state of Florida leaving an almost collapsed citrus industry (3) and it has already spread, with potential similar consequences, to other important citrus producing states such as California and Texas (48).

HLB Symptomatology

HLB early development is characterized by vein yellowing and an asymmetrical chlorosis in leaves known as “blotchy mottle”, symptom easily confused with mineral deficiencies such as those of zinc, iron, and manganese (2). Early symptoms of yellowing may appear on a single shoot or branch. As the disease develops, infected shoots are stunted, and the branches gradually die (2).

Infected trees are generally stunned, display twig dieback and have a sparse yellow foliage. The yellowing usually spreads throughout the tree over a year, especially on young trees, causing the productivity to decline within a few years (2). Root systems of infected trees are often poorly developed and new root growth may be suppressed (3). Infected fruit are small, lopsided, and have a bitter taste. Many fruits fall prematurely, while those that keep on the tree do not color properly, remaining green on the shaded side (49). Inside the fruits, the seeds are aborted, have a smaller size and show a dark coloration (4).

At the histological level, HLB symptoms are observed as a middle lamella swelling between cell walls surrounding sieve elements, and the deposition of amorphous callose in the sieve elements (50). This callose deposition lead to a reduction of the size of the sieve pore that interferes with photo assimilates transport from the leaves to the sink organs, and results in a starch accumulation in the chloroplasts (51). Thus, overall HLB symptoms are attributed to this disruption of the phloem function, that results in plant root decline, reduced photosynthesis, and reduced nutrient transportation (3).

Economic impact of HLB in the US

HLB economically impacts the citrus production by increasing the tree mortality rate, reducing the marketable yield per tree and by rising cost production (52). Just in Florida, HLB associated estimated losses rounded the 1.7 billion losses in the first five years, while the value of Florida citrus production decreased by $4.51 billion between 2006-07 and 2010-11 (53). From 2006 to 2011, more than 6611 people have lost their jobs in orange juice manufacturers due to HLB, with total losses in revenue of $3.63 billion (53). A recent report of the National Academies of Sciences, Engineering, and Medicine declared an effective management program for HLB in the next future is improbable and estimated a cumulative loss of 374 million per year in grower revenues from 2007 to 2014 (54).

HLB disease Management

The control of this disease is especially difficult due to the high dependence of it causal agents on both, their vector insect and plant hosts (48). In places where HLB is not present, the implementation of quarantine measures is the best way to avoid the introduction and dissemination of the pathogen (3). After the initial detection of the pathogen and at low incidence levels the use of insecticides and the eradication of the infected trees is the most effective way to eliminate HLB (55). However, factors such as the occurrence of asymptomatic infections, the long incubation period of the disease, and the fact that infected mature trees can still produce marketable fruits for several years, made this measure economically inefficient (52).

Several initiatives have been taken in order to cure HLB infected trees. One of the most widely tested has been the application of antimicrobials (52). Antibacterial compounds such as β-

lactams, Tetracyclines and Aminoglycosides have been tested with more or less efficacy to control the disease, but these methods faced issues such as phytotoxicity, the presence of antibiotic residues in the fruit and a high cost labor (56). Other chemical compounds that stimulate the plant vigor and the plant response to CLas have been used to mitigate HLB caused symptoms, however an extensive study performed by Gottwald et al. (57) demonstrated the failure of these methods to reduce CLas titers in infected plants, and showed no significant increases in plant health and fruit quality after these treatments.

Thermotherapy has been extensively tested in order to reduce CLas titers in HLB infected trees (48). In this method, infected plants are exposed to temperatures above 40°C with differences in duration and treatment repetition, and has been used in combination with antimicrobial compounds (58). Heat treatments were effective reducing CLas titers in infected citrus plants in potted plants (59) and in green house trials (48). However, when applied in mature plants the field, this method did not eradicate CLas population (59), and its generalized use outside the greenhouse is still economically inviable (21).

The situation in Florida is critical, the pathogen has already spread to other major citrus production areas, and an effective management program for HLB seems improbable (54). In the specific scenario of high incidence of Florida, it is imperative the application of methods that effectively reduce CLas population on mature infected trees, and subsequently reduce the transmission of the pathogen to new planted healthy trees.

Zinc oxide nanoparticles as antimicrobial compounds

In the last couple of decades, nanoparticles (NPs) have been extensively studied and have found practical applications in a variety of areas that include chemistry, engineering, physics, biology, and medicine (60). In drug delivery systems, the use of nanomaterials have brought a wide spectrum of forms with improved physicochemical characteristics and curative properties (61). Among them, Zinc oxide (ZnO) NPs represent an important class of commercially material and has been widely applied in diagnostics, therapeutics, drug-delivery systems, and food additives, among other fields, due to their magnetic, catalytic, semiconducting, antimicrobial, and binding properties (62).

The antimicrobial activity of these compounds rely on new characteristics that result from the reduction of their particle size (61). As the dimensions of the metal oxide is reduced, the specific surface area in contact with the solution is increased (63), and a greater number of radicals groups remain located on the NP surface which induce biochemical catalysis (64).

The most important antibacterial mechanisms for ZnO nanoparticles is the production of reactive oxygen species (ROS) (65). Radicals hydroxyl (OH^-), peroxide (H_2O_2) and superoxide (O_2^{2-}) adsorbed in the ZnO nanoparticle surface, are a main source of oxidative stress for bacterial cells (66). Hydrogen peroxide is the only cell permeable of these species and can penetrate to the cell where it binds and destroys nucleic acids, lipids and proteins (67). Superoxide and hydroxyl radicals, on the other side, cannot penetrate into the membrane due to their negative charges, but accumulate in the bacterial outer membranes from where can enhance cell permeability, disrupt proton motive force and generate cell wall damage due to ZnO

localized interaction, among other processes (67). Another proposed mode of action for ZnO NP is the production of cell membrane damage due to the direct contact of the harsh surface of the NP with the bacterial surface. The presence of uneven surface texture due to rough edges and corners makes ZnO NP more abrasive than bulk ZnO (66). Thus, the interaction of ZnO NP and bacterial cell surfaces result in cell deformation and in most of the cases in disruption of the cell membrane, triggering morphological changes and membrane leakage (68). Other discussed mechanisms include the poisoning of bacteria due to the release of Zn ions in the media, and the reduction of bacterial growth due to the increase of electrostatic forces in the cell membrane (69).

Zinkicide™ as a chemical control candidate for HLB

Zinkicide™, is a novel nano-formulated ZnO compound designed with the goal to control bacterial citrus diseases (70). This compound was already tested in vitro against other model bacterial species such as *Xanthomonas citri* subsp. *citri, Escherichia coli and X. alfalfae subsp. citrumelonis* and it displayed a twofold lower minimum inhibitory concentration in vitro (MIC) than copper-based compounds (70). In initial field trials, the application of Zinkicide™ caused a significate reduction on Citrus Canker incidence compared with the untreated control plants and traditional copper based compounds (70). The market value of Zinkicide™ is estimated to be similar as regular copper-based antimicrobial compounds, therefore the inclusion of this compound in HLB management programs will not imply and additional cost for growers. All these characteristics make of this compound a promising product to test against CLas.

Overall hypothesis:

Zinkicide^{TM} causes a significative reduction in the planktonic growth and biofilm formation of *Liberibacter crescens*.

Main objective:

To evaluate the effect *in vitro* of the commercial formulation of Zinkicide^{TM} on growth, viability, and biofilm formation of *Liberibacter crescens*.

Specific objective 1: To identify the cultural factors that induce *Liberibacter crescens* biofilm formation *in vitro*, in batch cultures and microfluidic chambers.

Specific hypothesis 1: Lcr biofilm formation *in vitro* depends on the culture media formulation.

Specific objective 2: To evaluate the preventive and curative activity of the commercial formulation of Zinkicide^{TM} against the planktonic growth and biofilm formation of *Liberibacter crescens*, in batch cultures and microfluidic chambers.

Specific hypothesis 2: The commercial formulation of Zinkicide^{TM} significantly reduces the planktonic growth and the biofilm formation of *Liberibacter crescens.*

References

1. Fagen JR, Leonard MT, Coyle JF, McCullough CM, Davis-Richardson AG, Davis MJ, Triplett EW. 2014. *Liberibacter crescens* gen. nov., sp. nov., the first cultured member of the genus *Liberibacter*. Int J Syst Evol Microbiol 64:2461–2466.

2. Wang N, Trivedi P. 2013. Citrus Huanglongbing: A Newly Relevant Disease Presents Unprecedented Challenges. Phytopathology 103:652–665.

3. Wang N, Pierson EA, Setubal JC, Xu J, Levy JG, Zhang Y, Li J, Rangel LT, Martins J. 2017. The *Candidatus* Liberibacter–Host Interface: Insights into Pathogenesis Mechanisms and Disease Control. Annu Rev Phytopathol 55:451–482.

4. Gottwald TR, Bassanezi RB, Paulo S. 2007. Citrus Huanglongbing : The Pathogen and Its Impact Plant Health Progress Plant Health Progress.

5. Garnier M, Danel N BJ. 1984. Aetiology of citrus greening disease. Ann Microbiol 135A:169–179.

6. Deng X ling, Gao Y di, Chen J chi, Pu X lian, Kong W wen, Li H ping. 2012. Curent Situation of "*Candidatus* Liberibacter asiaticus" in Guangdong, China, Where Citrus Huanglongbing Was First Described. J Integr Agric 11:424–429.

7. Duan Y, Zhou L, Hall DG, Li W, Doddapaneni H, Lin H, Liu L, Vahling CM, Gabriel DW, Williams KP, Dickerman A, Sun Y, Gottwald T. 2009. Complete Genome Sequence of Citrus Huanglongbing Bacterium, "*Candidatus* Liberibacter asiaticus" Obtained Through Metagenomics. Mol Plant-Microbe Interact 22:1011–1020.

8. Wang L, Hu C, Shao L. 2017. The antimicrobial activity of nanoparticles: Present situation and prospects for the future. Int J Nanomedicine 12:1227–1249.

9. Leonard MT, Fagen JR, Davis-Richardson AG, Davis MJ, Triplett EW. 2012. Complete genome sequence of *Liberibacter crescens* BT-1. Stand Genomic Sci 7:271–283.

10. Weinert MP, Jacobson SC, Grimshaw JF, Bellis GA, Stephens PM, Gunua TG, Kame MF, Davis RI. 2004. Detection of Huanglongbing (citrus greening disease) in Timor-Leste (East Timor) and in Papua New Guinea. Australas Plant Pathol 33:135–136.

11. Wulff NA, Zhang S, Setubal JC, Almeida NF, Martins EC, Harakava R, Kumar D, Rangel LT, Foissac X, Bové JM, Gabriel DW. 2014. The Complete Genome Sequence of "*Candidatus* Liberibacter americanus", Associated with Citrus Huanglongbing. Mol Plant-Microbe Interact 27:163–176.

12. Lin H, Pietersen G, Han C, Read DA, Lou B, Gupta G, Civerolo EL. 2015. Complete Genome Sequence of "*Candidatus* Liberibacter africanus," a Bacterium Associated with Citrus Huanglongbing. Genome Announc 3:e00733-15.

13. Garnier M, Jagoueix-eveillard S, Cronje PR, Roux HF Le, Bove JM. 2018. Genomic characterization of a liberibacter present in an ornamental rutaceous tree , Calodendrum capense , in the Western Cape province of South Africa . Proposal of "*Candidatus* Liberibacter africanus subsp . capensis " 2119–2125.

14. Wang J, Haapalainen M, Schott T, Thompson SM, Smith GR, Nissinen AI, Pirhonen M. 2017. Genomic sequence of "*Candidatus* Liberibacter solanacearum" haplotype C and its comparison

with haplotype A and B genomes. PLoS One 12:1–21.

15. Thompson S, Fletcher JD, Ziebell H, Beard S, Panda P, Jorgensen N, Fowler S V, Liefting LW, Berry N, Pitman AR. 2013. First report of "*Candidatus* Liberibacter europaeus" associated with psyllid infested Scotch broom 5197.

16. Rascoe J, Kumagai LB, Woods P H V. 2017. "*Candidatus* Liberibacter crescens" detected in citrus. J Citrus Pathol 35.

17. Liefting LW, Perez-Egusquiza, Clover GRG. 2008. A New "*Candidatus* Liberibacter" Species in Solanum tuberosum in New Zealand. Plant Dis 92:1474.

18. Hansen AK, Trumble JT, Stouthamer R, Paine TD. 2008. A new huanglongbing species, "*Candidatus* liberibacter psyllaurous," found to infect tomato and potato, is vectored by the psyllid Bactericera cockerelli (Sulc). Appl Environ Microbiol 74:5862–5865.

19. Munyaneza and V. G. Sengoda JE. 2009. First Report of "*Candidatus* Liberibacter solanacearum" in Pepper Plants in México. Plant Dis 97:1376.

20. Aguilar E, Sengoda VG, Bextine B, McCue KF, Munyaneza JE. 2013. First report of "*Candidatus* Liberibacter solanacearum" on tobacco in Honduras. Plant Dis 97:1376.

21. Munyaneza JE, Sengoda VG, Stegmark R, Arvidsson a K, Anderbrant O, Yuvaraj JK, Ramert B, Nissinen A. 2012. First Report of "*Candidatus* Liberibacter solanacearum" Associated with Psyllid-Affected Carrots in Sweden. Plant Dis 96:453.

22. Teresani GR, Bertolini E, Alfaro-Fernández A, Martínez C, Tanaka FAO, Kitajima EW, Roselló M, Sanjuán S, Ferrándiz JC, López MM, Cambra M, Font MI. 2014. Association of "*Candidatus* Liberibacter solanacearum" with a Vegetative Disorder of Celery in Spain and Development of a Real-Time PCR Method for Its Detection. Phytopathology 104:804–811.

23. Murphy AF, Cating RA, Goyer A, Hamm PB, Rondon SI. 2014. First Report of Natural Infection by "*Candidatus* Liberibacter solanacearum" in Bittersweet Nightshade (Solanum dulcamara) in the Columbia Basin of Eastern Oregon 1:1–2.

24. Thinakaran J, Pierson E, Kunta M, Munyaneza JE, Rush CM, Henne DC. 2015. Silverleaf Nightshade (Solanum elaeagnifolium), a Reservoir Host for "*Candidatus* Liberibacter solanacearum", the Putative Causal Agent of Zebra Chip Disease of Potato. Plant Dis 99:910–915.

25. Hajri A, Loiseau M, Cousseau-Suhard P, Renaudin I, Gentit P. 2017. Genetic Characterization of "*Candidatus* Liberibacter solanacearum" Haplotypes Associated with Apiaceous Crops in France. Plant Dis 101:1383–1390.

26. Alvarado VY, Odokonyero D, Duncan O, Mirkov TE, Scholthof HB. 2012. Molecular and Physiological Properties Associated with Zebra Complex Disease in Potatoes and Its Relation with *Candidatus* Liberibacter Contents in Psyllid Vectors 7.

27. Babu B, Paret ML, Dufault N, Harmon CL. 2015. "*Candidatus* Liberibacter solanacearum ": An Emerging Pathogen Infecting Potato and Tomato 1. PP320 Plant Pathol Dep UF/IFAS Ext.

28. Fisher T, Vyas M, He R, Nelson W, Cicero J, Willer M, Kim R, Kramer R, May G, Crow J, Soderlund C, Gang D, Brown J. 2014. Comparison of Potato and Asian Citrus Psyllid Adult and Nymph Transcriptomes Identified Vector Transcripts with Potential Involvement in Circulative, Propagative *Liberibacter* Transmission. Pathogens 3:875–907.

29. Thomas MH, Alvarez S, Rohrig E. 2016. Citrus Greening Disease (Huanglongbing) in Florida :

Economic Impact , Management and the Potential for Biological Control 5:109–118.

30. Rashed A, Workneh F, Paetzold L, Gray J, Rush CM. 2014. Zebra chip disease development in relation to plant age and time of "*Candidatus* Liberibacter solanacearum" infection. Plant Dis 98:24–31.

31. Ammar ED, Shatters RG, Hall DG. 2011. Localization of *Candidatus* Liberibacter asiaticus, Associated with Citrus Huanglongbing Disease, in its Psyllid Vector using Fluorescence in situ Hybridization. J Phytopathol 159:726–734.

32. Sengoda VG, Buchman JL, Henne DC, Pappu HR. 2018. "*Candidatus* Liberibacter solanacearum" Titer Over Time in Bactericera cockerelli (Hemiptera : Triozidae) After Acquisition From Infected Potato and Tomato Plants 1964–1972.

33. Canale MC, Tomaseto AF, Haddad M de L, Della Coletta-Filho H, Lopes JRS. 2017. Latency and Persistence of "*Candidatus* Liberibacter asiaticus" in Its Psyllid Vector, Diaphorina citri (Hemiptera: Liviidae). Phytopathology 107:264–272.

34. Ghanim M, Achor D, Ghosh S, Kontsedalov S, Lebedev G, Levy A. 2017. "*Candidatus* Liberibacter asiaticus" Accumulates inside Endoplasmic Reticulum Associated Vacuoles in the Gut Cells of Diaphorina citri. Sci Rep 1–9.

35. Sengoda VG, Cooper WR, Swisher KD, Henne DC, Munyaneza JE. 2014. Latent Period and Transmission of "'*Candidatus*Liberibacter solanacearum'" by the Potato Psyllid Bactericera cockerelli (Hemiptera : Triozidae) 9:1–10.

36. Ukuda-hosokawa R, Sadoyama Y, Kishaba M, Kuriwada T, Anbutsu H. 2015. Infection Density Dynamics of the Citrus Greening Bacterium "*Candidatus* Liberibacter asiaticus " in Field Populations of the Psyllid Diaphorina citri and Its Relevance to the Efficiency of Pathogen 81:3728–3736.

37. Cicero JM, Fisher TW, Brown JK. 2016. Localization of " *Candidatus* Liberibacter solanacearum" and Evidence for Surface Appendages in the Potato Psyllid Vector. Phytopathology 106:142–154.

38. Ghanim M, Fattah-Hosseini S, Levy A, Cilia M. 2016. Morphological abnormalities and cell death in the Asian citrus psyllid (Diaphorina citri) midgut associated with *Candidatus* Liberibacter asiaticus. Sci Rep 6:1–11.

39. Kruse A, Fattah-Hosseini S, Saha S, Johnson R, Warwick ER, Sturgeon K, Mueller L, Maccoss MJ, Shatters, RG, Heck MC. 2017. Combining'omics and microscopy to visualize interactions between the Asian citrus psyllid vector and the Huanglongbing pathogen *Candidatus* Liberibacter asiaticus in the insect gut. PLoS One 12:1–28.

40. Vyas M, He R, Nelson W, Yin G, Cicero JM, Willer M, Kim R. 2018. Asian Citrus Psyllid Expression Profiles Suggest "*Candidatus* Liberibacter asiaticus"-Mediated Alteration of Adult Nutrition nd Metabolism, and of Nymphal Development and Immunity. PLoS One 10:1–20.

41. Lai KK, Davis-Richardson AG, Dias R, Triplett EW. 2016. Identification of the genes required for the culture of *Liberibacter crescens*, the closest cultured relative of the Liberibacter plant pathogens. Front Microbiol 7:1–11.

42. Lin H, Gudmestad NC. 2013. Aspects of Pathogen Genomics, Diversity, Epidemiology, Vector Dynamics, and Disease Management for a Newly Emerged Disease of Potato: Zebra Chip. Phytopathology 103:524–537.

43. Fleites LA, Jain M, Zhang S, Gabriel DW. 2014. "*Candidatus* Liberibacter asiaticus" prophage

late genes may limit host range and culturability. Appl Environ Microbiol 80:6023–6030.

44. Loto F, Coyle JF, Padgett KA, Pagliai FA, Gardner CL, Lorca GL, Gonzalez CF. 2017. Functional characterization of LotP from *Liberibacter* asiaticus. Microb Biotechnol 10:642–656.

45. Jain M, Fleites LA, Gabriel DW. 2017. A Small Wolbachia Protein Directly Represses Phage Lytic Cycle Genes in "*Candidatus* Liberibacter asiaticus" within Psyllids. mSphere 2:e00171-17.

46. Halbert SE, Niblett C, Manjunath KL, Lee RF, Brown LG. 2000. Establishment of two new vectors of citrus pathogens in Florida. Proc Int Soc Citric IX Congr 13:1016–1017.

47. Anonymous. 2008. FEDERAL DOMESTIC QUARANTINE ORDER : CITRUS GREENING DISEASE (CG) and ASIAN CITRUS PSYLLID (ACP), p. 1–6. *In* Plant Protection Act of June 20, 2000, Section 412(a).

48. Blaustein RA, Lorca GL, teplitski max. 2017. Challenges for Managing *Candidatus* Liberibacter spp. (Huanglongbing disease pathogen): Current Control Measures and Future Directions. Phytopathology PHYTO-07-17-0260-RVW.

49. Graca J. 1991. CITRUS GREENING DISEASE. Annu Rev Phytopathol 109–36.

50. Zou H, Gowda S, Zhou L, Hajeri S, Chen G, Duan Y. 2012. The Destructive Citrus Pathogen , "*Candidatus* Liberibacter asiaticus" Encodes a Functional Flagellin Characteristic of a Pathogen-Associated Molecular Pattern. PLoS One 7.

51. Koh E, Zhou L, Williams DS. 2012. Callose deposition in the phloem plasmodesmata and inhibition of phloem transport in citrus leaves infected with "*Candidatus* Liberibacter asiaticus ." Protoplasma 687–697.

52. Farnsworth D, Grogan KA, Bruggen AHC Van, Moss CB. 2014. The Potential Economic Cost and Response to Greening in Florida Citrus. Choices 29:1–6.

53. Hodges AW, Spreen TH. 2012. Economic impacts of citrus greening (HLB) in Florida, 2006/07-2010/11. EDIS FE903:1–6.

54. Committee on a Review of the Citrus Greening Research and Development Efforts. 2018. A Review of the Citrus Greening Research and Development Efforts Supported by the Citrus Research and Development Foundation: Fighting a Ravaging Disease. Natl Acad Press.

55. Monzo C, Stansly PA. 2018. Economic injury levels for Asian citrus psyllid control in process oranges from mature trees with high incidence of huanglongbing. PLoS One 12:1–13.

56. Munir S, He P, Wu Y, He P, Khan S, Huang M, Cui W, He P, He Y. 2017. Huanglongbing Control: Perhaps the End of the Beginning. Microb Ecol 1–13.

57. Gottwald TR, Graham JH, Irey MS, Mccollum TG, Wood BW. 2012. Inconsequential effect of nutritional treatments on huanglongbing control , fruit quality , bacterial titer and disease progress. Crop Prot 36:73–82.

58. Yang C, Powell CA, Duan Y, Shatters R, Fang J, Zhang M. 2018. Deciphering the Bacterial Microbiome in Huanglongbing-Affected Citrus Treated with Thermotherapy and Sulfonamide Antibiotics. PLoS One 11:1–9.

59. Doud MM, Wang Y, Hoffman MT, Latza CL, Luo W, Armstrong CM, Gottwald TR. 2017. Solar thermotherapy reduces the titer of *Candidatus* Liberibacter asiaticus and enhances canopy growth by altering gene expression pro fi les in HLB-affected citrus plants. Hortic Res 4.

60. Zaman M, Ahmad E, Qadeer A, Rabbani G, Khan RH. 2014. Nanoparticles in relation to peptide and protein aggregation. Int J Nanomedicine 9:899–912.

61. Dizaj SM, Lotfipour F, Barzegar-Jalali M, Zarrintan MH, Adibkia K. 2014. Antimicrobial activity of the metals and metal oxide nanoparticles. Mater Sci Eng C 44:278–284.

62. Choi SJ, Choy JH. 2014. Biokinetics of zinc oxide nanoparticles: Toxicokinetics, biological fates, and protein interaction. Int J Nanomedicine 9:261–269.

63. Espitia PJP, Soares N de FF, Coimbra JS dos R, de Andrade NJ, Cruz RS, Medeiros EAA. 2012. Zinc Oxide Nanoparticles: Synthesis, Antimicrobial Activity and Food Packaging Applications. Food Bioprocess Technol 5:1447–1464.

64. Dayem AA, Hossain MK, Lee S Bin, Kim K, Saha SK, Yang GM, Choi HY, Cho SG. 2017. The role of reactive oxygen species (ROS) in the biological activities of metallic nanoparticles. Int J Mol Sci 18:1–21.

65. Stanković A, Dimitrijević S, Uskoković D. 2013. Influence of size scale and morphology on antibacterial properties of ZnO powders hydrothemally synthesized using different surface stabilizing agents. Colloids Surfaces B Biointerfaces 102:21–28.

66. Padmavathy N, Vijayaraghavan R. 2008. Enhanced bioactivity of ZnO nanoparticles: An antimicrobial study. Sci Technol Adv Mater 9.

67. Sirelkhatim A, Mahmud S, Seeni A, Kaus NHM, Ann LC, Bakhori SKM, Hasan H, Mohamad D. 2015. Review on zinc oxide nanoparticles: Antibacterial activity and toxicity mechanism. Nano-Micro Lett 7:219–242.

68. Swain P, Nayak SK, Sasmal A, Behera T, Barik SK, Swain SK, Mishra SS, Sen AK, Das JK, Jayasankar P. 2014. Antimicrobial activity of metal based nanoparticles against microbes associated with diseases in aquaculture. World J Microbiol Biotechnol 30:2491–2502.

69. Zhang L, Ding Y, Povey M, York D. 2008. ZnO nanofluids: A potential antibacterial agent 18:939–944.

70. Graham JH, Johnson EG, Myers ME, Young M, Rajasekaran P, Das S, Santra S. 2016. Potential of Nano-Formulated Zinc Oxide for Control of Citrus Canker on Grapefruit Trees. Plant Dis 100:2442–2447.

Chapter 2: *Liberibacter crescens*, the only culturable member of its genus, forms biofilm under specific culture conditions

Abstract

Biofilm formation by pathogenic *Liberibacter* spp. have been observed in insect vectors, but not in planta so far. In order to assess the ability of *Liberibacter crescens* (Lcr), as a biological model for the genus, to form biofilms in vitro, media optimization was performed by manipulating concentrations of methyl-β-cyclodextrin (mβc) and fetal bovine serum (FBS) in media BM7. An initial modified medium (mBM7) where FBS was replaced by mβc at 1g/l was conducive for cell attachment to surfaces and biofilm formation, but yield lower overall growth in comparison to BM7. FBS concentration was positively correlated with total and planktonic growth and negatively correlated with biofilm formation. mβc concentration was positively correlated with biofilm formation when cells were pre-grown in mBM7 but no trend was observed when Lcr was pre-grown in BM7. The use of the alamarBlue® cell proliferation kit confirmed that mβc stimulates Lcr viability regardless of the initial medium used and showed Lcr viability was inversely correlated with biofilm formation. Cell adhesion force assays in microfluidic chambers (MC) confirmed that the BSA contained in the FBS fraction of the BM7 medium, prevents cell-surface attachment, and demonstrated that Lcr-surface attachment does not rely on protein synthesis. Cell-cell aggregation assays showed Lcr aggregated more in the optimized media formulation for biofilm formation (mBM7) than in BM7. Microscopic characterization of floating and attached Lcr cell aggregates showed Lcr biofilms are embedded in an EPS extracellular matrix, and that surface-attached biofilms are formed on the flask bottom. Time-lapse microscopy assays in microfluidic chambers showed Lcr cells divide more actively on the center of the microcolony than on the edges. Based in

our observations, we hypothesize Lcr biofilm formation is triggered by stress, as a survival response mechanism to unfavorable environmental conditions. This may explain why pathogenic *Liberibacter* spp. only form biofilms in the unique extracellular stage of their life cycle.

Introduction

Liberibacter species are the causal agents of devastating plant diseases worldwide that include Huanglongbing (HLB) or citrus greening and Zebra Chip of potato (1, 2). HLB is a centenary disease that was officially first described in the coastal Chaoshan Plain of Guangdong Province, China in the late 19th century and is currently a serious threat to major citrus producing area worldwide (1, 3). In the US, the disease was first detected in 2005 in Florida and since then it has seriously impacted US citrus industry with around $300 million loses per year, the elimination of dozens of thousands of commercial citrus trees and the loss of more than 8,000 jobs (4). HLB is associated with three different species that include '*Candidatus* Liberibacter asiaticus' (CLas) and '*Candidatus* Liberibacter americanus' (CLam), which are vectored by the Asian citrus psyllid (ACP) *Diaphorina citri*, and a third species, '*Ca.* L. africanus' (CLaf), transmitted by the African citrus psyllid *Trioza erytreae* (2). Zebra Chip is a newly emerged disease associated with '*Candidatus* Liberibacter solanacearum' (CLso) (5, 6). Since its first detection in tomato and potato, CLso has been reported causing vegetative disorders in pepper (7), tobacco (8), carrot (8), celery (9), bittersweet (10), Silverleaf Nightshade (*Solanum elaeagnifolium*) (11), and more recently in chervil, fennel, parsley, and parsnip (12). In 2009 this disease was prevalent in most potato-producing states in the US, and reached epidemic levels in

2011 in the Pacific Northwest states (13). These major pathogenic species share specific features that makes them difficult to study: first, all pathogenic *Liberibacter* spp. are insect-vectored, and second, all of them have a phloem-limited and intracellular lifestyle inside their plant hosts. These characteristics make these pathogens strictly dependent on their hosts, hitherto unculturable in vitro, and difficult to control by conventional methods. (14).

Liberibacter crescens (Lcr) is the only culturable species of the *Liberibacter* genus. This bacterium was isolated from the phloem sap of a defoliating mountain papaya in Puerto Rico in 2008 (15). The lack of fulfilment of Koch's postulates, or even infecting specific plant hosts, precludes the classification of Lcr as a plant pathogen, but it has been described as a phloem limited bacterium as its pathogenic close relatives (15). Interestingly, a recent report based in a multilocus sequence typing approach, identified a new ´*Candidatus* Lcr´ infecting several hosts of the Rutaceae family including kumquat (*Citrus japonica*) and curry (*Bergera koenigii*) showing blotchy mottle symptoms (16). Despite the lack of proof Lcr pathogenicity, the ability to cultivate Lcr in vitro makes of this species the best biological model to study and predict unculturable *Liberibacter* spp. biology. Hence, Lcr has been used as a valuable tool for studies in *Liberibacter* spp. comparative genomics (15, 17, 18, 6) and heterologous expression of CLas genes (19–21).

Biofilms are assemblages of microorganisms attached to a solid surface and encased in an extracellular polymeric matrix (22). These surface-associated bacterial biofilm communities are widespread in all types of natural environments, and are more abundant in nature than the individualized planktonic bacteria (23). To date, no biofilm formation has been described for pathogenic *Liberibacter* spp. inside their plant host. However, fluorescence in-situ hybridization studies targeting CLas cells on the digestive system of

infected psyllids, have shown this pathogen undergoes an extensive surface colonization forming cell aggregates previous to intracellular movement and circulative transmission (24, 25). Confirming these observations, gene expression profile comparison between infected and uninfected *Diaphorina citri* and *Trioza eritreae* insects, demonstrated an overexpression of cell adhesion and biofilm formation-related genes during vector insect midgut colonization, suggesting the biofilm formation process is a critical step during vector colonization and subsequent circulative transmission (26).

In this study we demonstrated the capacity of Lcr to attach to surfaces, form cell-cell aggregates and produce an EPS extracellular matrix in batch cultures and under flow conditions, all main features of a natural biofilm forming bacteria. Based in previous studies and in our observations, we suggest Lcr biofilm formation is triggered as a mechanism to cope with unfavorable environmental conditions, hypothesis that may explain why *Liberibacter* spp. only forms biofilms in the unique extracellular stages of their life cycles. The study of biofilm formation process in Lcr as a model for *Liberibacter* spp., has a remarkable importance to better understand the biological interactions on these insect vectored-plant pathogenic systems with their environment and consequently, for the design of novel strategies to mitigate the impact of these deleterious organisms.

Materials and Methods

Bacterial strains

Liberibacter crescens strain BT-1 (27) was used for this study. BT-1 Lcr strains were grown on BM7 agar solid medium at 28°C from cryo-conservation vials for 7-8 days and then streaked in a second passage in BM7 for another 6 days, previous to conduct each experiment. A GFP-Lcr BT1 strain, gently donated by Dr. Dean Gabriel, from the Institute of Food and Agricultural Sciences, University of Florida, was used for microscopic analysis of Lcr floating cell aggregates. GFP-Lcr strains were grown on BM7 agar solid medium supplemented with 4.5µg/ml of kanamycin, at 28°C from cryo-conservation vials for 7-8 days, and then streaked in a second passage in the same medium formulation for another 6 days, previous to experiment performance.

Media formulations

Main media formulation recipes tested in this work are summarized in the Table 2-1. A basal medium consisting on BM7 (27) without the fetal bovine serum (FBS) fraction and completed to the final volume with sterile deionized water (bBM7, of basal BM7), was used for used for Lcr bacterial suspension preparation and designated as a blank for subsequent media optimization. An initial conducive modified media (mBM7) was prepared by supplementing the bBM7 with 1g/l of methyl-β-cyclodextrin (mβc) (SIGMA-ALDRICH, St. Louis, MO. USA). The selection of this concentration value was based in previous studies that demonstrated the effective replacement of FBS by this compound when culturing other intracellular fastidious bacteria (28). FBS (Hyclone, South Logan,

Utah. USA) concentration gradients where prepared by manipulating the volume fractions of this compound and water added to the bBM7 formulation, while mβc gradients were prepared by increasing the mass of this reagent on the same basal medium. The final mBM7 formulation, with 0.75g/l of mβc, resulted from the optimum Lcr cell viability and biofilm formation determined for this media. A last formulation, bBM7+BSA, resulted from adding 3.5g of bovine serum albumin (BSA) to the bBM7 media.

Table 2-1. Formulation for 1L of the main media used in this work.

Reagent	**bBM7**	**BM7**	**mBM7**	**bBM7+BSA**
Molecular-grade water	700ml	550ml	700ml	700ml
Alpha-ketoglutaric acid	2g	2g	2g	2g
ACES buffer	10g	10g	10g	10g
Potassium hydroxide	3.75g	3.75g	3.75g	3.75g
TNM-FH insect medium	300ml	300ml	300ml	300ml
FBS	-	150ml	-	-
methyl-β-cyclodextrin	-	-	0.75g	-
BSA	-	-	-	3.5g

bBM7: basal BM7; **mBM7:** modified BM7

Media optimization for biofilm formation

Optimal mβc and FBS concentration values for total, planktonic and biofilm growth were determined in polystyrene 96 well plates (COSTAR®, Kennebunk, ME. USA) starting from both BM7 and mBM7 agar plates. Wells placed at the plate edges of the 96 well plates were initially filled with 250µl of sterile deionized water to avoid the effect of desiccation. Then, 10µl of the Lcr bacterial suspension in bBM7 (OD_{600nm}=1) was inoculated onto 190µl of bBM7 supplemented with mβc concentration gradient from 0 to 1g/l (0.25g/l increments). Similarly, in an independent experiment, BM7 media without the FBS fraction, was completed to the final volume with increasing FBS concentration values to reach final concentration values of 3, 6, 9, 12 and 15% on each media

formulation. Treatments were inoculated with Lcr bacterial suspensions as described above. Six blank wells and six Lcr cultures replicates were included for each treatment. The experiments were repeated 2 times independently. Plates were wrapped with parafilm and incubated at 28°C and 150rpm for 8 days. Total growth curves for each treatment were built by daily turbidity assessment at 600nm (OD_{600}), using a Cytation 3 Image Reader spectrophotometer (BioTek Instruments Inc, Winooski, Vermont, USA). In a second set of experiments, late exponential phase cultures (6dpi) in the same treatments described above were used for total, planktonic and biofilm growth quantification. Total and planktonic growth were determined by turbidity as described above, while biofilm formation was quantified using a crystal violet assay (29). Blank absorbance values were subtracted from absolute total and biofilm growth values for each treatment. Significant differences in planktonic growth for the mβc concentration gradient assays started from BM7 were determined by a Student-Newman-Keuls Method. For the biofilm fraction the statistical analysis was performed by a Fisher-LSD method, while differences for the total growth were calculated by a multiple comparison using a Dunn's method. Differences in planktonic and total growth for mβc gradients started from mBM7 were determined by a Fisher-LSD method. For the biofilm fractions the differences between the treatments were calculated using a Student-Newman-Keuls Method. Differences on the total, biofilm and planktonic growth of the all FBS gradient assays were determined by a Fisher-LSD method. All the statistical analyses were performed using the SIGMA Plot Software, Version 11.0 at a significance level of $P < 0.05$.

Cell viability assay

Due to inconsistencies in Lcr culture turbidity in absence of FBS in polystyrene 96 well plates caused by Lcr cell attachment to the side walls, the alamarBlue® cell proliferation and viability reagent (Bio-Rad Laboratories Inc, Hercules, CA. USA.) was used as a complementary method to assess Lcr total growth/viability for each mβc concentration value. The alamarBlue® cell viability kit allows colorimetric detection of cellular metabolic reduction and is suitable for eukaryote and prokaryote cells. Its chromophore active compound is cell diffusible and detects cell proliferation for both the suspended and attached cell fractions, hence we selected it to quantify overall Lcr cell proliferation in a unified value. Briefly, Lcr cultures were inoculated in a mβc concentration gradient as previously described and incubated for six days at 28°C, 150rpm. Then, 20µl of alamarBlue® was added to Lcr cultures and allowed to incubate for four additional hours under the same growth conditions. To avoid cell interference with the absorbance readings, each plate was centrifuged at 4000 rpm for 10 min and 150µl of the cell free supernatant was transferred to a fresh plate. Absorbance measurements were performed at 600 and 570nm wavelengths for each replicate using a Cytation 3 Image Reader spectrophotometer (BioTek Instruments Inc, Winooski, Vermont, USA). Lcr viability on each mβc concentration value was assessed as the average alamarBlue® percentage reduction (ABPR) for four replicates per treatment, following the absorbance-based method as described in the manufacturer instructions. Experiments were repeated twice independently. Significant differences among treatments cell viability values were determined using an Fisher Least Significant Difference (LSD) method for the assays pre-cultured in mBM7, and by the Kruskal-Wallis One Way Analysis of Variance on Ranks

for the assays started from BM7, at a significance level of $P < 0.05$ for both tests, using the SIGMA Plot Software, Version 11.0. The medium formulation with the mβc concentration value that displayed the optimum Lcr biofilm formation and cell viability, was used as the modified culture (mBM7) for subsequent experiments.

Strength of bacterial surface attachment in microfluidic chambers

Lcr cell attachment force for bBM7, BM7, mBM7 and bBM7+BSA media was assessed in MC as previously described (30). In order to determine if Lcr cell attachment relies on active protein synthesis, the mBM7 media formulation was supplemented with 100µg/ml of the protein synthesis inhibitor agent tetracycline (SIGMA-ALDRICH, St. Louis, MO. USA) and was also assessed for attachment force as beforehand tested (31). Significant differences between cell attachment registered for each media formulation was determined calculated by the Fisher LSD One Way ANOVA method, at the significance level $P < 0.05$, using the SIGMA Plot Software, Version 11.0.

Microscopic characterization of Lcr cell-cell aggregates and surface attached biofilms

Microscopic Lcr biofilm characterization was performed in 24 well plates (VWR International, LLC, PA. USA). As described for other non-motile facultative anaerobes, it was expected that Lcr will form biofilms at the bottom of the culture flasks (32–34)**.** In order to collect biofilms from the bottom of the cultures, 0.8 x 0.8 cm glass pieces were cut from borosilicate cover glass slides (Fisherbrand®, Pittsburng, PA. USA), autoclave-sterilized for 15min and dried for 30 min at 80°C. After cooling, the glass pieces were aseptically placed at the bottom of sterile polystyrene 24 well. Then, 2ml of Lcr cultures

in BM7 and mBM7 (OD_{600nm}=0.5), were inoculated by quadruplicate for each media formulation and incubated at 28 ºC and 150 rpm for eight days. In another experiment set, 2ml of GFP-Lcr cultures in BM7 and mBM7 (OD_{600nm}=0.5), were inoculated by quadruplicate for each media formulation and incubated under the same conditions. After the incubation time, 1ml of the liquid of both experiment sets cultures was carefully removed without disturbing the settled cell aggregates and all the cultures were observed under a Zeiss Stemi 508 stereo microscope (Göttingen, Germany) at 10X magnification. Images were captured with a Carl Zeiss GmbH microscopy camera (Göttingen, Germany) controlled by the ZEN lite software (Carl Zeiss Microscopy GmbH, Jena. Germany). Then, 1ml pipette tip was cut in the thinner extreme and cell clumps formed in the bottom of the cultures of the GFP-Lcr strain, were carefully transferred altogether with 1ml of culture medium to a well in a fresh plate. Then, 10µl of Calcofluor white (St. Louis, MO. USA) and 10 µl of KOH 10% was added and incubated for 5 minutes in the dark. After staining, the cell clumps were recovered with sterile tweezers without disrupting them, and sandwiched between two borosilicate coverslips. Image analysis was performed using a Nikon Eclipse A1 confocal laser scanning microscope (Nikon, Melville, NY) using a 60X oil immersion objective. To detect cells and EPS, excitation wavelengths of 528 and 590nm were used, respectively. To characterize attached biofilms, each glass slide-containing well with the wild-type Lcr strain, was gently washed three times and finally resuspended in 2ml of sterile deionized water. Then 6µl of an equal volume mix of both reagents of the LIVE/DEAD® BactLight Bacterial Viability Kit (Invitrogen, Eugene, OR. USA) were added, 24 well plates were wrapped in aluminum foil and incubated at 150rpm at 28°C for 15min. After incubation time, 10µl of Calcofluor white (St. Louis, MO. USA) and 10µl of KOH 10% were added and incubated for additional 5 minutes

under the same conditions. Then each slide piece was placed on top of a borosilicate slide with the biofilm facing up. A drop of water was added over the attached biofilms to maintain the three-dimensional (3D) structure and to avoid desiccation. Image analysis was performed using a Nikon Eclipse A1 confocal laser scanning microscope (Nikon, Melville, NY) using a 40X distance objective. To detect all three of the dyes used, (propidium iodide, SYTO 9, and calcofluor white), excitation wavelengths of 528, 590, and 370 nm, respectively, were used. To analyze the 3D structure of the biofilm, 1µm interval z-series were automatically captured in a deep range of 25µm. Images were acquired with a CoolSnap HQ2 camera (Photometrics, Tucson, AZ) and processed with NIS-Elements AR software, version 3.0 (Nikon, Melville, NY).

Lcr biofilm formation in microfluidic chambers (MC).

Pathogenic *Liberibacter* spp. live under flow conditions inside their plant hosts and vector insects, for this reason, the Lcr biofilm formation process was assessed in a microfluidic chamber system resembling their natural habitat (30). Microfluidic chamber design and fabrication was performed as previously described (30). The channels were initially filled with mBM7 using an automated syringe pump (Pico Plus; Harvard Apparatus, Holliston, MA). Lcr bacterial suspensions in mBM7 (OD_{600nm}=0.5) were injected for one hour to obtain attached cells. After a critical number of attached cells was observed (>10 cells/100µm^2), bacterial cultures inlets were clamped with surgical scissors, and the flow rate of the media was maintained constant at 0.25µl/min for two weeks. The MC was mounted onto a Nikon Eclipse Ti inverted microscope (Nikon, Melville, NY) and observed with a 40X objective using phase contrast and Nomarski differential interference contrast (DIC) optics. Cell division over time was recorded using time-lapse video

imaging microscopy. Image acquisition was performed automatically every 10min using a Nikon DS-Q1 digital camera (Nikon, Melville, NY) controlled by NIS- Elements software version 3.0 (Nikon, Melville, NY). At least three independent experiments were performed. Lcr cell viability inside MC was assessed the LIVE/DEAD® BactLight Bacterial viability kit. Briefly, 3µl of each reagent of the kit was added to 1ml of mBM7, loaded into a 1ml plastic syringe (BD Becton Dickinson, Utah, USA), aseptically interchanged by the culture media in the microfluidic chamber and inoculated at the same flow rate used above overnight. To detect both dyes used, (propidium iodide and SYTO 9), excitation wavelengths were used as described above.

Results

Cultural factors influencing Lcr growth viability and biofilm formation

FBS concentration positively correlated with Lcr total and planktonic growth regardless of the initial growth media used (Table 2-2). The optimum FBS value for Lcr total and planktonic growth was observed at 15% of the serum in the experiments started from BM7 and no significant differences were observed between 12 and 15% for experiments started from mBM7 (Fig 2-1-A, C). The presence of FBS drastically suppressed Lcr biofilm growth at all the concentration tested with no significant differences among the concentration values tested (Fig 2-1-C, D). mβc concentration slightly increased planktonic growth in experiments starting from mBM7, with optimum values between 0.5 and 0.75g/l with no significant differences between the treatments (Fig 2-2-B). For the biofilm fraction growth, a marked numerical and statistically significant difference was

observed at 0.75 g/l of mβc for experiments started from mBM7 (Fig 2-2-D), while variable and mostly no significant differences are observed for treatments started from BM7 (Fig 2-2-C). A similar trend for the total and planktonic Lcr growth was observed for mβc concentration gradients for cultures started from BM7.

Cell viability assays showed that ABPR was positively correlated with mβc concentration below 0.75g/l regardless the media formulation where Lcr was previously grown (Fig 2-3) (Table 2-4). No significant differences were observed for ABPR values above 0.25g/l for trials started from BM7 (Fig 2-3-A) while for assays started from mBM7 significant differences for all the concentration tested with an optimum value at 0.75g/l, and a significant decrease was recorded at 1g/l (Fig 2-3-B). The representation of the ratios for each growth fraction showed the biofilm growth/planktonic growth ratio was the highest at the lowest ABPR values for both experiments while the planktonic growth/biofilm growth ratio followed a similar trend that the viability values.

Adhesion force experiments showed Lcr attached strongest in absence of FBS and mβc in the bBM7 medium (Fig 2-4-A, B). Average adhesion force vales were 740.25 ±11 pN for bBM7, 715.03 ± 15pN for mBM7 and 714.80 ± 23pN for mBM7 supplemented with tetracycline, with no significant differences between the treatments (Fig 2-4-B). No Lcr attached cells were obtained with the lowest flow rate when inoculated in BM7 or bBM7+BSA confirming BSA blocks Lcr cell-surface attachment (Fig 2-4-A, B).

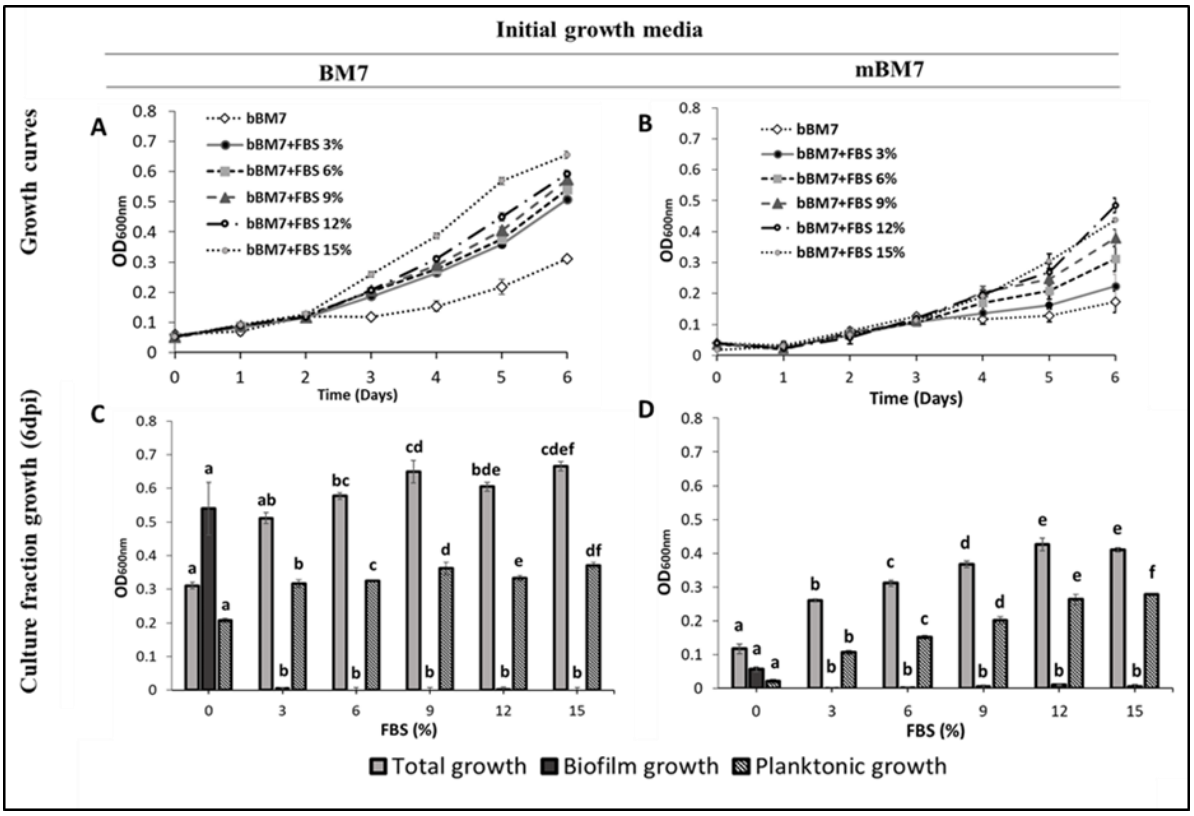

Figure 2-1. Lcr growth in FBS concentration gradients. A) and B) Lcr growth curves on FBS concentration gradients started from BM7 and mBM7 agar plates respectively. C) and D) Lcr total, planktonic and biofilm growth values (n=6) on each FBS concentration value at 6dpi started from BM7 and mBM7 agar plates respectively. Different letters on bars correspond to statistical significant differences at $P < 0.05$. Error bars: standard deviations. Experiments were repeated 2 times, and one representative experiment is shown.

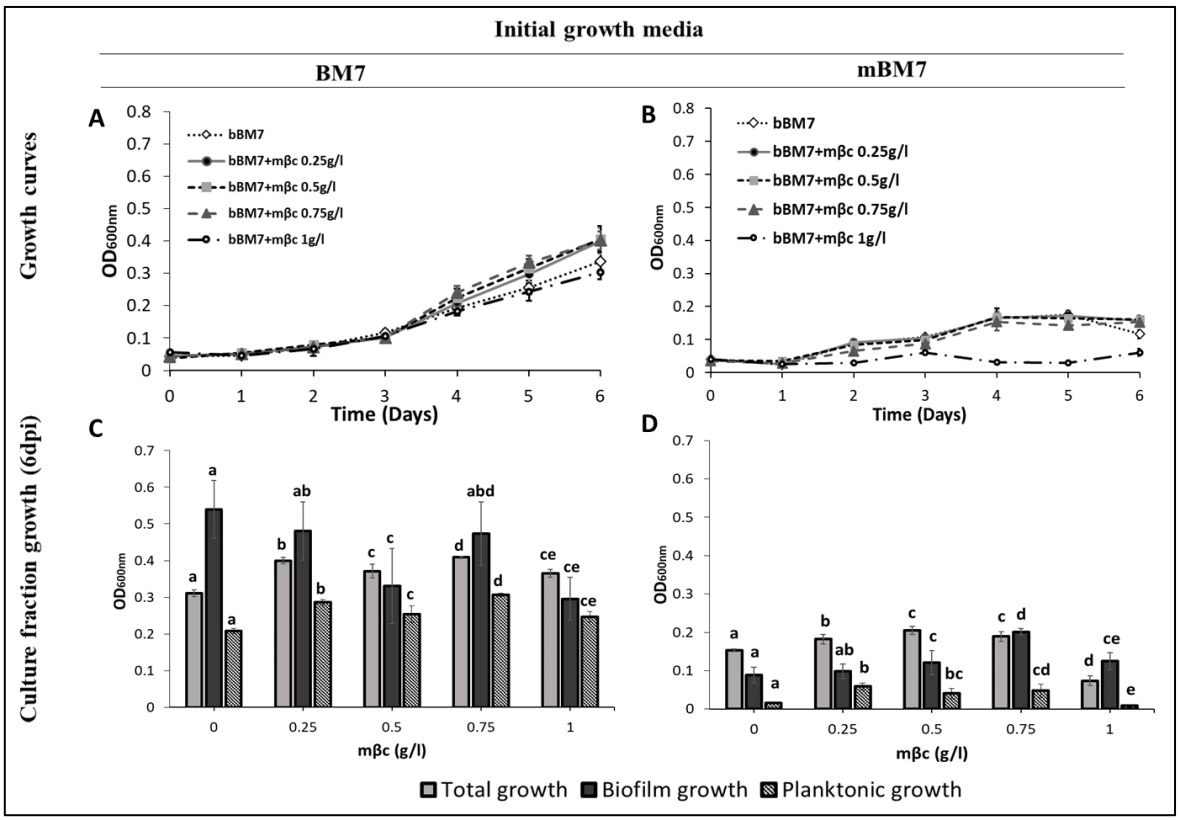

Figure 2-2. Lcr growth in mβc concentration gradients. A) and B) Lcr growth curves on mβc concentration gradients started from BM7 and mBM7 agar plates respectively. C) and D), Lcr total, planktonic and biofilm growth values (n=6) on each mβc concentration value at 6dpi started from BM7 and mBM7 agar plates respectively. Different letters on bars correspond to statistical significant differences at $P < 0.05$. Error bars: standard deviations. Experiments were repeated 2 times, and one representative experiment is shown.

Table 2-2. Pearson r coefficient values for the linear regression analysis between each culture fraction quantified at 6dpi and FBS concentration values.

Initial growth media	Variables	Pearson r coeff.
BM7	Total growth/FBS conc.	0.87
	Planktonic growth/FBS conc.	0.82
	Biofilm growth /FBS conc.	-0.66
mBM7	Total growth/FBS conc.	0.94
	Planktonic growth/FBS conc.	0.99
	Biofilm growth/FBS conc.	-0.54

Table 2-3. Pearson r coefficient values for the linear regression analysis between each culture fraction quantified at 6dpi and mβc concentration values from 0 to 0.75g/l.

Initial growth media	Variables	Pearson r coeff.
BM7	Total growth/mβc conc.	0.77
	Planktonic growth/mβc conc.	0.79
	Biofilm growth/mβc conc.	-0.50
mBM7	Total growth/mβc conc.	0.78
	Planktonic growth/mβc conc.	0.55
	Biofilm growth/mβc conc.	0.91

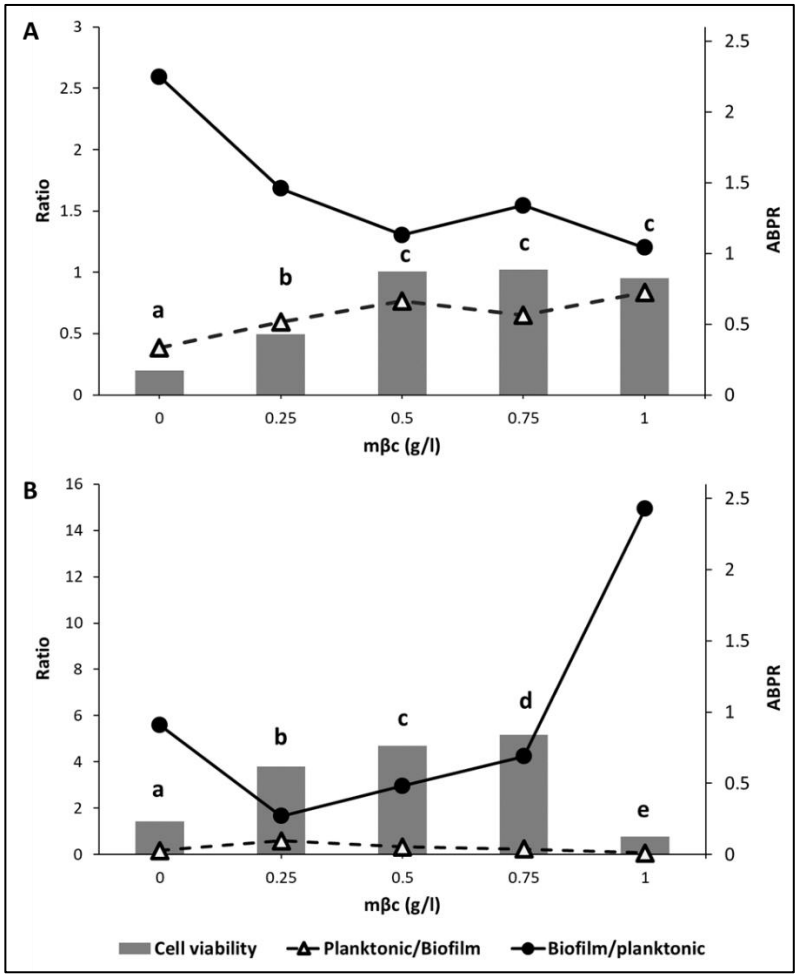

Figure 2-3. Lcr cell viability and culture fraction ratios variation in response to different mβc concentrations. A) Cultures started from BM7. B) Cultures started from mBM7. Right axes: alamarBlue® percentage reduction (ABPR) values. Left axes: Ratio values. The bar chart represents the average ABPR values (n=4) for each culture condition at 6dpi. The different letters on the bar chart shown in A) correspond to statistical significant differences according to a Kruskal-Wallis One Way Analysis of Variance on Ranks test results ($P < 0.05$). The different letters on the bar chart shown in B) correspond to statistical significant differences according to LSD test results ($P < 0.05$). Lcr biofilm/planktonic ratio were obtained by dividing the average biofilm growth by the average planktonic growth for each mβc concentration. Lcr planktonic/biofilm ratio were

obtained by dividing the average biofilm growth by the average planktonic growth for each mβc concentration.

Table 2-4. Pearson r coefficent values for the linear regresion analysis between each culture fraction quantified at 6dpi and the ABPR obtained for each mβc concentration value from 0 to 0.75g/l.

Initial growth media	Variables	Pearson r coeff.
BM7	ABPR/mβc conc.	0.95
	ABPR/Total growth	0.68
	ABPR/Planktonic growth	0.65
	ABPR/Biofilm growth	-0.74
mBM7	ABPR/mβc conc.	0.94
	ABPR/Total growth	0.92
	ABPR/Planktonic growth	0.75
	ABPR/Biofilm growth	0.73

The characterization of Lcr cell-cell aggregates showed qualitative differences on each media formulation. After a week of incubation, Lcr formed cloud-like cell aggregates in the bottom of the wells of all the mBM7 treatments that were visible with the naked eye (Fig 2-5-B), while a fine layer of settled cells was observed in BM7 (Fig 2-5-A). The staining of these cell aggregates from both cultures (BM7 and mBM7) with Calcofluor white showed the presence of EPS in both media formulations, but displayed Lcr formed bigger and more compact cell aggregates in mBM7 (Fig 2-5-D). In BM7, EPS stained by calcofluor white seemed more diffuse and cells easily dislodge from the cell aggregates when covered with the coverslip (Fig 2-5-C). On the other hand, cell aggregates collected from mBM7 medium showed a more compact structure after placing them in a glass sandwich, and EPS and cells were forming a gel-like compact structure (Fig 2-5-D).

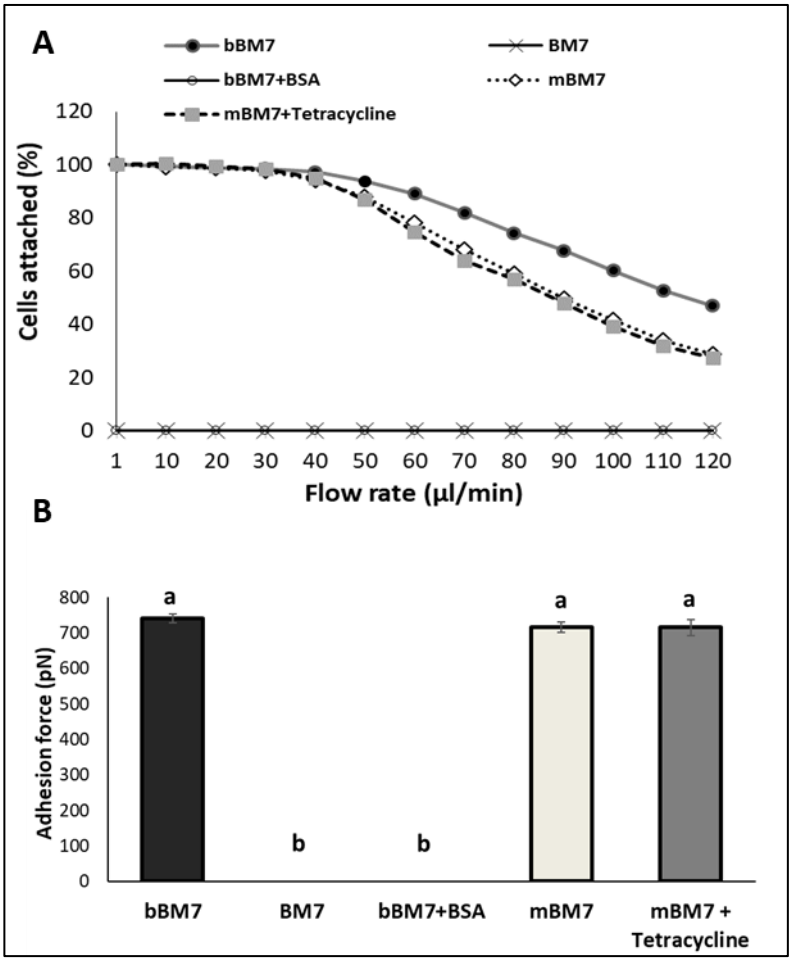

Figure 2-4. Lcr attachment force assessment in MC. A) Average numbers of Lcr cells attached to the microfluidic chamber surface (n>5) as a function of the flow rate for each culture treatment. B) Adhesion force of Lcr for each media formulation. The different letters on the bars correspond to statistical significant differences according to a Fisher-LSD test results ($P < 0.05$). Error bars: standard deviations.

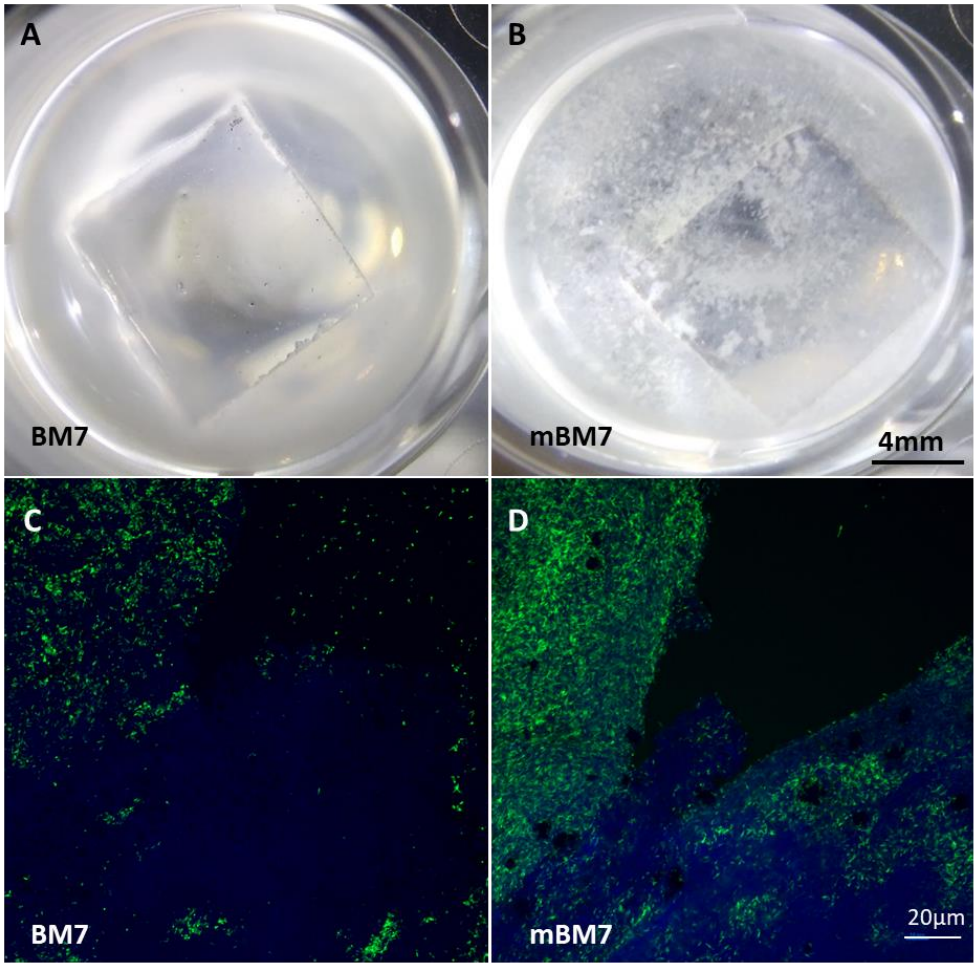

Figure 2-5. Characterization of GFP-Lcr floating biofilms in batch cultures by CLSM at 7dpi. Macroscopic appearance of Lcr cultures in BM7 (A) and mBM7 (B). Microscopic appearance of Lcr cultures in BM7 (C) and mBM7 (D). GFP-Lcr cells are emitting green fluorescence; EPS are stained in blue.

Lcr biofilm characterization in batch cultures

The 3D characterization of 7-day old biofilms in mBM7 revealed a cake-like structure (Fig 2-6-A) formed by cells attached to the lower surface better observed from the bottom view (Fig 2-6-E) and an EPS layer covering and popping out from the cell aggregates (Fig 2-6-A, B). EPS-naked small cell clusters of live cells were also observed isolated in a minor proportion than EPS embedded biofilms (Fig 2-6-A). Live cells were predominant in Lcr biofilm at this time (Fig 2-5-C), while dead cells whether extracellular DNA, where mostly found in clusters localized in small amounts the cell-EPS interface (Fig 2-5-A, D). Lcr biofilms scored a maximum deep higher than 25μm in the EPS popping areas (Fig 2-5-F).

Lcr biofilm formation in MC

In MC assays, Lcr cells were observed mostly in pairs after initial cell attachment. After 24-48hrs microcolonies started growing in several directions by an initial cell elongation followed by and incomplete cell division keeping cells closely attached. After the initial surface expansion cells divided more actively from the center of the microcolony, shown by more refractory cell aggregates in the center of the microcolony, while a lower activity was observed in the cells growing at the edges (Fig 2-7-A). No visible extracellular matrix was observed using the bright field during the two weeks of culture under flow conditions, but big cell aggregates were formed from the lateral inlets (Fig 2-7-B) after 10 days. The visual screening of cell viability revealed a high proportion of live cells in Lcr biofilms formed under flow conditions in the microfluidic chamber (Fig 2-6-C). For more details please refer to the supplementary Video 1.

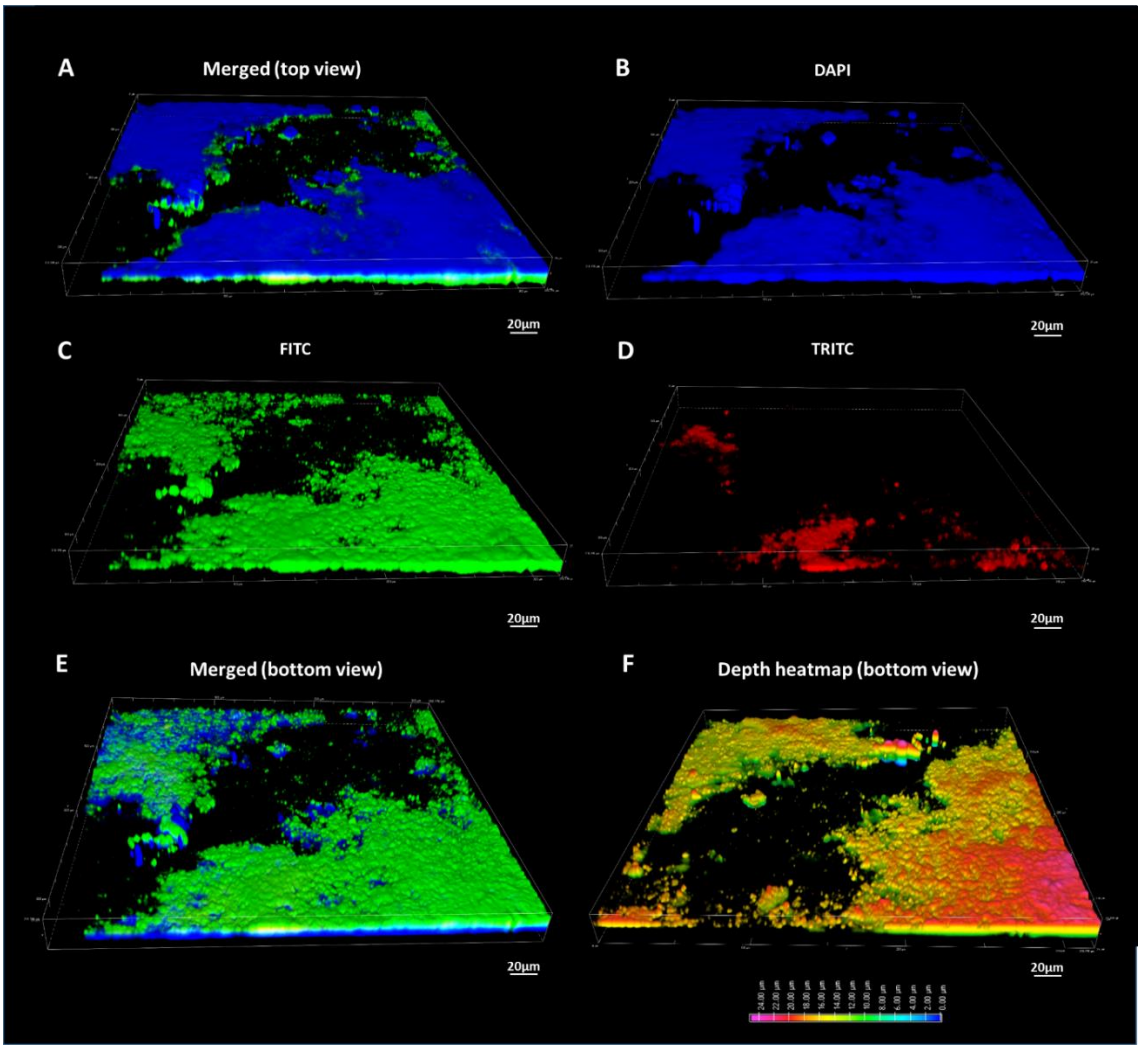

Figure 2-6. Three-dimensional characterization of Lcr attached biofilms by CLSM. A) Merged image of the top view B) EPS stained in blue (DAPI filter). C) Live cells stained green (FITC filter). D) Dead cells stained in red (TRITC filter). E) Merged image of the bottom view. F) Depth heat map.

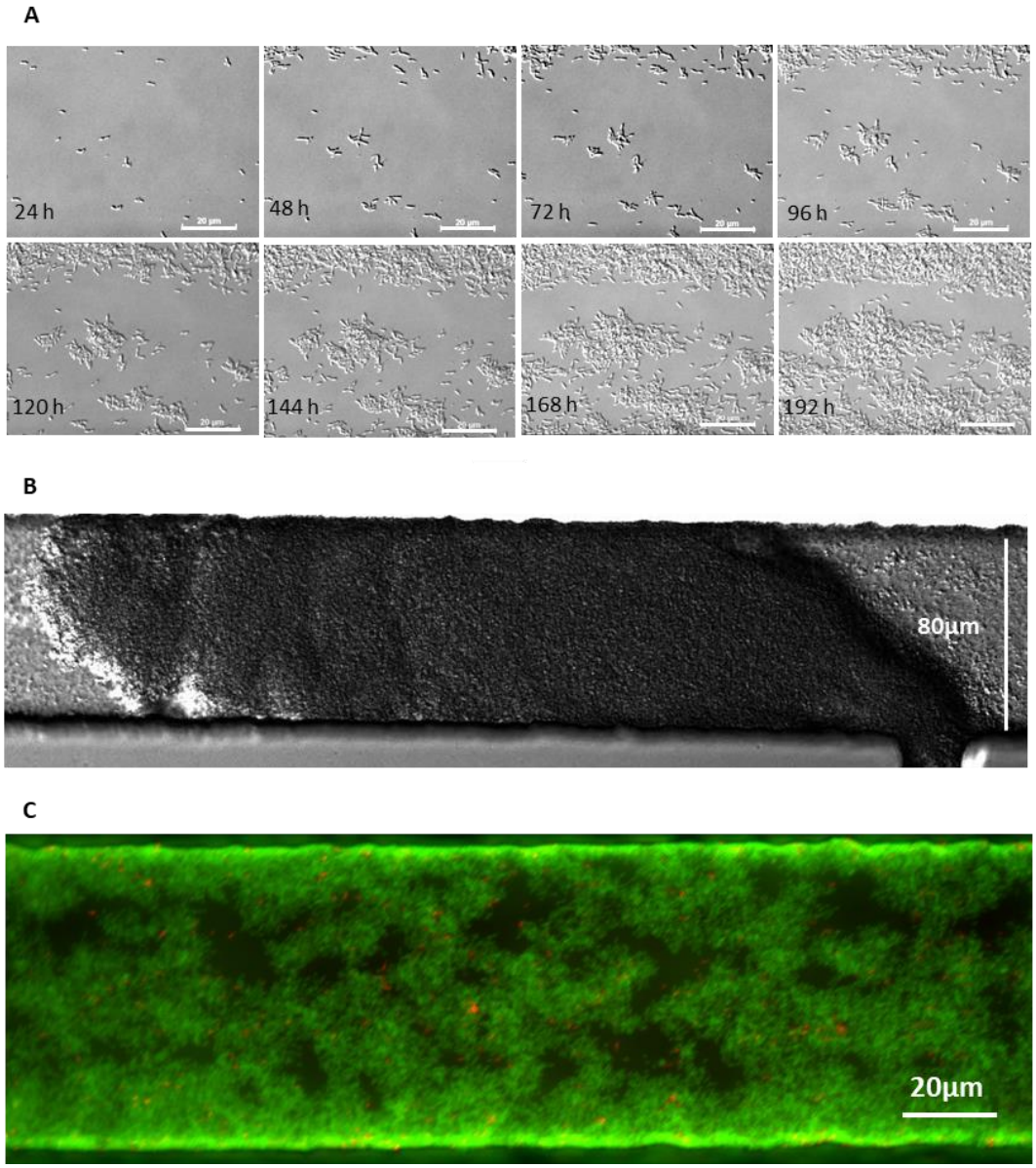

Figure 2-7. Microscopic characterization of Lcr biofilms in MC. A) Lcr microcolony development under flow conditions. Scale bar, 20µm. B) Lcr floating cell aggregate rising from the lateral inlet of the microfluidic chamber 15dpi. Scale bar, 80µm. C) Viability of Lcr cells in microfluidic chambers determined with the Live/Dead cell viability kit and examination by inverted fluorescence microscopy at 7dpi. Scale bar, 20µm.

Discussion

Biofilm formation in *Liberibacter* spp. has been suggested inside their vector insect supported by culture independent methods such as fluorescent *in-situ* hybridization of the target *Liberibacter* species inside the vector insect (35, 36), and predictions based in gene expression analysis (26). However, no fulfillment for the biofilm definition has been completed for these microorganisms, due to the destructive nature of these methods and culturable limitations. In this work, we demonstrated that Lcr i) attaches to solid surfaces, ii) forms cohesive cell aggregates and iii) these cells aggregates are embedded in a polymeric extracellular matrix. At the same time, we observed an inverse correlation between changes in cell viability and biofilm formation that suggest that general stress induces Lcr biofilm formation. Finally, we evaluated and optimized this process in microfluidic chambers, bringing a valuable approach for future studies in a system that better resemble the natural environment where these pathogens inhabit.

Initial cell-surface attachment is the first step in the biofilm development cycle, and is essential for subsequent colonization and biofilm formation (37–39). In this work we demonstrated that the presence of the globular protein BSA in the culture media blocked Lcr cell-surface attachment and therefore suppressed biofilm formation. Several authors have exploited this dependence on the media composition to avoid the initial adhesion process in bacteria (40). For instance, Privet et al. (41) exponentially reduced the adhesion of *Staphylococcus aureus* and *Pseudomonas aeruginosa* to surfaces by coating a hydrophobic xerogel as antiadhesive agent, while Alugupalli & Kalfas (42) demonstrated lactoferrin inhibit the adhesion of *Actinobacillus actinomycetemcomitans*, *Prevotella intermedia* and *P. nigriscens* to fibroblast monolayers and reconstituted basement

membranes. Specifically BSA, is a well-known blocking agent used in enzyme-based immunoassays to avoid non-specific interactions between biomolecules and solid surfaces (43, 44) and it is proved it reduces the biofilm formation of *Pseudomonas aeruginosa* on plastic surfaces and intravenous catheters (45) and blocks the bacterial surface adhesion of *Staphylococcus aureus* and *S. intermedius* to impedimetric gold electrodes (46). Since the BSA is one of the predominant compounds in the FBS, and we proved its antiadhesive properties in MC assays and batch cultures at the concentration expected in the BM7 medium formulation, we conclude it is the main compound interfering with Lcr cell-surface attachment in this medium.

After media formulation modification, Lcr avidly adhered to several materials that include polystyrene, polycarbonate and polydimethylsiloxane (PDMS). In adhesion force assays in MC, Lcr recorded the highest adhesion force registered to the date using this method, for the three treatments we tested in absence of blocking agents. Previous studies in *Xylella fastidiosa* adhesion force in MC, reported the highest adhesion force for *pilB* mutants (strains with only Type I pili and no presence of Type IV pili) at 204 ± 22 pN (30) which is more than three-fold lower than *Lcr* adhesion force values registered in our assays. The overnight exposure of Lcr to 100µg/ml of the protein synthesis inhibitor tetracycline did not influence on Lcr cell-surface attachment force. Lcr sensibility to tetracycline was determined around 15µg/ml (15), therefore the exposure to such dose should disrupt the protein synthesis and subsequently the processes that rely on it. Previous experiments using this method for *X. fastidiosa* showed a significant reduction in cell-surface adhesion force when exposed to the same concentration of the antibiotic (31). For the model of *X. fastidiosa*, the cell-surface attachment process is mainly mediated by

surface appendages of proteinaceous nature such as type I and IV pili (29), therefore is expected the disruption of protein synthesis negatively impacts this process. However, and contrary to CLas and CLso also, Lcr genome does not codify for any known proteinaceous molecule involved in tight adherence (27). Based in the previous genomic data and the results we obtained in these experiments, we infer Lcr cell-surface attachment is not mainly governed by a protein surface interaction, and suggest that other cell membrane surface compounds such as lipopolysaccharides and/or EPS (47) may be mediating this process for this species.

Cultures started from BM7 showed a higher total, planktonic and biofilm growth for all the treatments tested in comparison to cultures comparisons started from mBM7 (Fig 2-1). Growth curves for each trial showed the use of mBM7 as initial culture medium severely modified Lcr growth dynamics by extending the lag phase, shortening the exponential phase and by a prematurely entrance in the stationary phase in all the treatment tested (Fig 2-1, 2-2). FBS is a complex chemical formulation that influences cell growth and proliferation by supplying transport proteins, essential nutrients, trace elements, and stabilizing and detoxifying factors needed for maintaining a favorable growth environment (48). The replacement of FBS with mβc mitigates in some extent, but does not fulfill, all the nutritional requirements for Lcr growth as the FBS does. Hence, Lcr grows nutritionally stressed in absence of FBS, and therefore, it requires a longer lag phase and shows a lower growth rate when transferred to a medium with optimum conditions.

AlamarBlue® cell viability assays showed mβc positively correlated with Lcr overall cell viability with an optimum concentration at 0.75g/l. A similar effect was already

demonstrated for this compound by Sandoz et al. who showed an increased viability over time and a reduction in the oxidative stress in axenic cultures of the intracellular pathogen *Coxiella burnetii* (28). Despite the effect of mβc on Lcr growth is not as marked as the FBS or BSA, its effect on Lcr viability stimulation, and its low cost compared to BSA, may be exploited for future attempts to bring unculturable *Liberibacter* spp. to pure culture in vitro.

Lcr biofilm formation at 6dpi was positively correlated with mβc when Lcr cultures where started from mBM7 agar plates but no clear trend was observed when cultures were started from BM7. However, the high biofilm formation levels registered, and the lack of significant differences between most of the treatments for biofilm formation on the experiments started from BM7, may indicate Lcr saturated its biofilm formation capacity at this time point, and probably entered in the final detachment phase. Sampling at earlier time may address the question if mβc is positively correlated with the biofilm formation at low cell densities or if the initial nutritional stage of the cells influences mβc effect in Lcr biofilm formation. Is also noticeable that cultures started from mBM7 registered the highest biofilm growth/planktonic growth ratios than those started from BM7. Apparently, nutritionally stressed Lcr cells grown in mBM7 are more prone to adhere to surfaces and form biofilm than nutritionally replete Lcr cells, pre-grown in BM7.

In this work we found that Lcr has higher cell aggregation when grown in mBM7 broth at 7dpi, which is the media that allows biofilm formation by this organism. When compared to other plant pathogens known to produce biofilm, such as *X. fastidiosa,* that aggregates in hours, Lcr aggregates in a lower rate and in a slower fashion (49). Factors as the absence of functional genes for motility in the reduced genome of Lcr (27) that speeds

cell-cell interaction and/or the absence of a chemical signal, may be the cause of this delay in cell-cell aggregation. Nevertheless, Lcr can form a measurable biofilm, which is accompanied by cell aggregation, a typical phenotypic characteristic of this structure.

The inspection of Lcr biofilms by CLSM, showed these structures are mostly formed at the bottom of the flasks. Lcr cell settling feature as result of cell-cell aggregation and it is non-motile nature combined with its high cell-surface attachment activity may contribute to biofilm formation in the lowest surfaces of the flaks. This characteristic is typical of nonmotile or motility defective bacteria (50) and has been described in well characterized biofilm forming bacteria such as *S. aureus* (32, 51) and *Clostridium perfringens* (33). The staining of Lcr biofilms and cell aggregates with Calcofluor white also showed Lcr cells are embedded in an EPS extracellular matrix. This structure protects the embedded cells against environmental stressing factors such as mechanical shear, predation, invasion, and antibiotics (52–55) and improves bacterial cell-cell and cell-surface adhesion (46). CLSM analysis of Lcr biofilms also showed Lcr dead cells are localized in clusters in the cell-EPS interface, while the bottom side is plenty formed by live cells. These dead cells are the main source of extracellular DNA for biofilm matrices, and the last, acts as a structural stabilizer, improves microbial adhesion and promotes bacterial horizontal gene transfer (56). This predominance of live cell in the bottom and the localization of dead cells close to the EPS matrix, together with and the more active cell division observed in the center of microcolonies may reflect a growth pattern for Lcr biofilms. In this growth model, Lcr youngest cells are generated in the center of the microcolony, while older and dead cells are displaced to the outer layers of the structure. Factors such as a more favorable environment in the sheltered interior of the biofilm and/or the production of a

cell density dependent chemical signal may be responsible for this active growth in the center of the microcolonies.

In our study, Lcr planktonic growth was higher in all mβc supplemented formulations compared with in the non-supplemented medium (Fig 2-2). Lcr cultures were always displaced to the biofilm formation under low viability conditions (Fig 2-4) and the biofilm growth/planktonic growth ratio was quite higher for cultures started from mBM7 (a nutritional depleted medium), compared to cultures pre-grown in BM7. This link between a stressing factor and biofilm formation in Lcr, suggest this process is triggered as a defense response to adverse conditions and may explain why *Liberibacter* spp. forms biofilm in the insect digestive system but not in the insect hemolymph of the plant phloem. Unculturable *Liberibacter* spp. thrive planktonically inside intracellular environments in both the plant host and the vector insect (1). In these systems, products of anabolism are predominant and degradative processes are minimized. On the other side, in the digestive system of the insect, enzymatic degradative processes are active and biofilm formation represents an adaptive advantage to cope with these catabolic processes in the surroundings. At the same time, the close interactions between insect cells and *Liberibacter* spp. facilitated by cell-surface attachment and cell-cell aggregation, alone with the microenvironment created inside the biofilm, may facilitate the endocytosis process necessary for the subsequent circulative transmission.

In summary, Lcr biofilm formation is a complex phenome that requires of the conjunction of several factor on each developmental stage. The study of this process in this species as a biological model for the entire genus, opens a new research field for these pathosystems,

and will help to better understand the interaction between these pathogens and their hosts, their vectors and the environment.

References

1. Wang N, Pierson EA, Setubal JC, Xu J, Levy JG, Zhang Y, Li J, Rangel LT, Martins J. 2017. The *Candidatus* Liberibacter–Host Interface: Insights into Pathogenesis Mechanisms and Disease Control. Annu Rev Phytopathol 55:451–482.

2. Wang N, Trivedi P. 2013. Citrus Huanglongbing: A Newly Relevant Disease Presents Unprecedented Challenges. Phytopathology 103:652–665.

3. Deng X ling, Gao Y di, Chen J chi, Pu X lian, Kong W wen, Li H ping. 2012. Curent Situation of "*Candidatus* Liberibacter asiaticus" in Guangdong, China, Where Citrus Huanglongbing Was First Described. J Integr Agric 11:424–429.

4. Hodges AW, Spreen TH. 2012. Economic impacts of citrus greening (HLB) in Florida, 2006/07-2010/11. EDIS FE903:1–6.

5. Liefting LW, Sutherland PW, Ward LI, Paice KL, Weir BS, Clover GRG. 2009. A New " *Candidatus* Liberibacter" Species Associated with Diseases of Solanaceous Crops. Plant Dis 93:208–214.

6. Lin H, Gudmestad NC. 2013. Aspects of Pathogen Genomics, Diversity, Epidemiology, Vector Dynamics, and Disease Management for a Newly Emerged Disease of Potato: Zebra Chip. Phytopathology 103:524–537.

7. Munyaneza and V. G. Sengoda JE. 2009. First Report of "*Candidatus* Liberibacter solanacearum" in Pepper Plants in México. Plant Dis 97:1376.

8. Munyaneza JE, Sengoda VG, Stegmark R, Arvidsson a K, Anderbrant O, Yuvaraj JK, Ramert B, Nissinen A. 2012. First Report of "*Candidatus* Liberibacter solanacearum" Associated with Psyllid-Affected Carrots in Sweden. Plant Dis 96:453.

9. Teresani GR, Bertolini E, Alfaro-Fernández A, Martínez C, Tanaka FAO, Kitajima EW, Roselló M, Sanjuán S, Ferrándiz JC, López MM, Cambra M, Font MI. 2014. Association of "*Candidatus* Liberibacter solanacearum" with a Vegetative Disorder of Celery in Spain and Development of a Real-Time PCR Method for Its Detection. Phytopathology 104:804–811.

10. Murphy AF, Cating RA, Goyer A, Hamm PB, Rondon SI. 2014. First Report of Natural Infection by "*Candidatus* Liberibacter solanacearum" in Bittersweet Nightshade (Solanum dulcamara) in the Columbia Basin of Eastern Oregon 1:1–2.

11. Thinakaran J, Pierson E, Kunta M, Munyaneza JE, Rush CM, Henne DC. 2015. Silverleaf Nightshade (Solanum elaeagnifolium), a Reservoir Host for "*Candidatus* Liberibacter solanacearum", the Putative Causal Agent of Zebra Chip Disease of Potato. Plant Dis 99:910–915.

12. Hajri A, Loiseau M, Cousseau-Suhard P, Renaudin I, Gentit P. 2017. Genetic Characterization of "*Candidatus* Liberibacter solanacearum" Haplotypes Associated with Apiaceous Crops in France. Plant Dis 101:1383–1390.

13. Babu B, Paret ML, Dufault N, Harmon CL. 2015. "*Candidatus* Liberibacter solanacearum ": An Emerging Pathogen Infecting Potato and Tomato 1. PP320 Plant Pathol Dep UF/IFAS Ext.

14. Li W, Hartung JS, Levy L. 2006. Quantitative real-time PCR for detection and identification of *Candidatus* Liberibacter species associated with citrus huanglongbing. J Microbiol Methods 66:104–115.

15. Fagen JR, Leonard MT, Coyle JF, McCullough CM, Davis-Richardson AG, Davis MJ, Triplett EW. 2014. *Liberibacter crescens* gen. nov., sp. nov., the first cultured member of the genus *Liberibacter*. Int J Syst Evol Microbiol 64:2461–2466.

16. Rascoe J, Kumagai LB, Woods P H V. 2017. "*Candidatus* Liberibacter crescens" detected in citrus. J Citrus Pathol 35.

17. Wang J, Haapalainen M, Schott T, Thompson SM, Smith GR, Nissinen AI, Pirhonen M. 2017. Genomic sequence of "*Candidatus* Liberibacter solanacearum" haplotype C and its comparison with haplotype A and B genomes. PLoS One 12:1–21.

18. Lai KK, Davis-Richardson AG, Dias R, Triplett EW. 2016. Identification of the genes required for the culture of *Liberibacter crescens*, the closest cultured relative of the Liberibacter plant pathogens. Front Microbiol 7:1–11.

19. Fleites LA, Jain M, Zhang S, Gabriel DW. 2014. "*Candidatus* Liberibacter asiaticus" prophage late genes may limit host range and culturability. Appl Environ Microbiol 80:6023–6030.

20. Loto F, Coyle JF, Padgett KA, Pagliai FA, Gardner CL, Lorca GL, Gonzalez CF. 2017. Functional characterization of LotP from *Liberibacter* asiaticus. Microb Biotechnol 10:642–656.

21. Jain M, Fleites LA, Gabriel DW. 2017. A Small Wolbachia Protein Directly Represses Phage Lytic Cycle Genes in "*Candidatus* Liberibacter asiaticus" within Psyllids. mSphere 2:e00171-17.

22. Kirisits MJ, Prost L, Starkey M, Parsek R, Parsek MR. 2005. Characterization of Colony Morphology Variants Isolated from Pseudomonas aeruginosa Biofilms Characterization of Colony Morphology Variants Isolated from Pseudomonas aeruginosa Biofilms. Appl Environ Microbiol 71:4809–4821.

23. Lebeaux D, Ghigo J-M, Beloin C. 2014. Biofilm-Related Infections: Bridging the Gap between Clinical Management and Fundamental Aspects of Recalcitrance toward Antibiotics. Microbiol Mol Biol Rev 78:510–543.

24. Ammar ED, Shatters RG, Hall DG. 2011. Localization of *Candidatus* Liberibacter asiaticus, Associated with Citrus Huanglongbing Disease, in its Psyllid Vector using Fluorescence in situ Hybridization. J Phytopathol 159:726–734.

25. Ghanim M, Fattah-Hosseini S, Levy A, Cilia M. 2016. Morphological abnormalities and cell death in the Asian citrus psyllid (Diaphorina citri) midgut associated with *Candidatus* Liberibacter asiaticus. Sci Rep 6:1–11.

26. Vyas M, He R, Nelson W, Yin G, Cicero JM, Willer M, Kim R. 2018. Asian Citrus Psyllid Expression Profiles Suggest "*Candidatus* Liberibacter asiaticus"-Mediated Alteration of Adult Nutrition nd Metabolism, and of Nymphal Development and Immunity. PLoS One 10:1–20.

27. Leonard MT, Fagen JR, Davis-Richardson AG, Davis MJ, Triplett EW. 2012. Complete genome sequence of *Liberibacter crescens* BT-1. Stand Genomic Sci 7:271–283.

28. Sandoz KM, Sturdevant DE, Hansen B, Heinzen RA. 2014. Developmental transitions of Coxiella burnetii grown in axenic media. J Microbiol Methods 96:104–110.

29. Zaini PA, De La Fuente L, Hoch HC, Burr TJ. 2009. Grapevine xylem sap enhances biofilm development by Xylella fastidiosa. FEMS Microbiol Lett 295:129–134.

30. De La Fuente L, Montanes E, Meng Y, Li Y, Burr TJ, Hoch HC, Wu M. 2007. Assessing adhesion forces of type I and type IV pili of Xylella fastidiosa bacteria by use of a microfluidic flow chamber. Appl Environ Microbiol 73:2690–2696.

31. Cruz LF, Cobine PA, De La Fuente L. 2012. Calcium increases Xylella fastidiosa surface attachment, biofilm formation, and twitching motility. Appl Environ Microbiol 78:1321–1331.

32. Stepanović S, Vuković D, Dakić I, Savić B, Švabić-Vlahović M. 2000. A modified microtiter-plate test for quantification of staphylococcal biofilm formation. J Microbiol Methods 40:175–179.

33. Charlebois A, Jacques M, Archambault M. 2014. Biofilm formation of Clostridium perfringens and its exposure to low-dose antimicrobials. Front Microbiol 5:1–11.

34. Curtis WR. 2014. Insights into Clostridium phytofermentans biofilm formation: aggregation, microcolony development and the role of extracellular DNA. Microbiology 160:1134–1143.

35. Cicero JM, Fisher TW, Brown JK. 2016. Localization of " *Candidatus* Liberibacter solanacearum" and Evidence for Surface Appendages in the Potato Psyllid Vector. Phytopathology 106:142–154.

36. Fisher T, Vyas M, He R, Nelson W, Cicero J, Willer M, Kim R, Kramer R, May G, Crow J, Soderlund C, Gang D, Brown J. 2014. Comparison of Potato and Asian Citrus Psyllid Adult and Nymph Transcriptomes Identified Vector Transcripts with Potential Involvement in Circulative, Propagative *Liberibacter* Transmission. Pathogens 3:875–907.

37. Chagnot C, Zorgani MA, Astruc T, Desvaux M. 2013. Proteinaceous determinants of surface colonization in bacteria: bacterial adhesion and biofilm formation from a protein secretion perspective. Front Microbiol 4:1–26.

38. Veerachamy S, Yarlagadda T, Manivasagam G, Yarlagadda PK. 2014. Bacterial adherence and biofilm formation on medical implants: A review. Proc Inst Mech Eng Part H J Eng Med 228:1083–1099.

39. Ofek I, Hasty DL, Sharon N. 2003. Anti-adhesion therapy of bacterial diseases: Prospects and problems. FEMS Immunol Med Microbiol 38:181–191.

40. Gupta P, Sarkar S, Das B, Bhattacharjee S, Tribedi P. 2016. Biofilm, pathogenesis and prevention—a journey to break the wall: a review. Arch Microbiol 198:1–15.

41. Benjamin J. Privett, Jonghae Youn, Sung A Hong, Jiyeon Lee, Junhee Han, Jae Ho Shin and MHS. 2011. Antibacterial Fluorinated Silica Colloid Superhydrophobic Surfaces 27:9597–9601.

42. Alugupalli KR KS. 1997. Characterization of the lactoferrin-dependent inhibition of the adhesion of Actinobacillus actinomycetemcomitans, Prevotella intermedia and Prevotella nigrescens to fibroblasts and to a reconstituted basement membrane. APMIS 105:680–8.

43. Jeyachandran YL, Mielczarski JA, Mielczarski E, Rai B. 2010. Efficiency of blocking of

non-specific interaction of different proteins by BSA adsorbed on hydrophobic and hydrophilic surfaces. J Colloid Interface Sci 341:136–142.

44. Kretzer J, Biebl M, Miller S. 2008. Sample preparation–an essential prerequisite for high-quality bacteria detectionPrinciples of bacterial detection: Biosensors, ….

45. Hammond A, Dertien J, Colmer-Hamood JA, Griswold JA, Hamood AN. 2010. Serum Inhibits P. aeruginosa Biofilm Formation on Plastic Surfaces and Intravenous Catheters. J Surg Res 159:735–746.

46. Riquelme M V., Zhao H, Srinivasaraghavan V, Pruden A, Vikesland P, Agah M. 2016. Optimizing blocking of nonspecific bacterial attachment to impedimetric biosensors. Sens Bio-Sensing Res 8:47–54.

47. Hori K, Matsumoto S. 2010. Bacterial adhesion: From mechanism to control. Biochem Eng J 48:424–434.

48. Fang CY, Wu CC, Fang CL, Chen WY, Chen CL. 2017. Long-term growth comparison studies of FBS and FBS alternatives in six head and neck cell lines. PLoS One 12:1–27.

49. Kandel PP, Almeida RPP, Cobine PA, De La Fuente L. 2017. Natural Competence Rates Are Variable Among *Xylella fastidiosa* Strains and Homologous Recombination Occurs In Vitro Between Subspecies *fastidiosa* and *multiplex*. Mol Plant-Microbe Interact 30:589–600.

50. O'Toole GA, Kolter R. 1998. Flagellar and twitching motility are necessary for Pseudomonas aeruginosa biofilm development. Mol Microbiol 30:295–304.

51. Stephanovic S, VUKOVIC D, HOLA V, BONAVENTURA G DI, DJUKIC S, IRKOVIC I, RUZICKA2 F. 2007. Quantification of Biofilm in Microtiter Plates: Overview of Testing Conditions and Practical Recommendations for Assessment of Biofilm Production by Staphylococci. Apmis 115:891–899.

52. Hou J, Veeregowda DH, van de Belt-Gritter B, Busscher HJ, van der Mei HC. 2018. Extracellular polymeric matrix production and relaxation under fluid shear and mechanical pressure in Staphylococcus aureus biofilms. Appl Environ Microbiol 84:1–14.

53. Solano C, Echeverz M, Lasa I. 2014. Biofilm dispersion and quorum sensing. Curr Opin Microbiol 18:96–104.

54. Cardenas E, Kranabetter JM, Hope G, Maas KR, Hallam S, Mohn WW. 2015. Forest harvesting reduces the soil metagenomic potential for biomass decomposition. ISME J 9:2465–2476.

55. Abdulamir AS, Jassim SAA, Hafidh RR, Bakar FA. 2015. The potential of bacteriophage cocktail in eliminating Methicillin-resistant Staphylococcus aureus biofilms in terms of different extracellular matrices expressed by PIA, ciaA-D and FnBPA genes. Ann Clin Microbiol Antimicrob 14:1–10.

56. Okshevsky M, Meyer RL. 2015. The role of extracellular DNA in the establishment, maintenance and perpetuation of bacterial biofilms. Crit Rev Microbiol 41:341–352.

Chapter 3: In vitro antimicrobial activity of a zinc-based nanoparticle compound, *Z*inkicide™, against *Liberibacter crescens*, as a biological model for pathogenic *Liberibacter* spp.

Abstract

HLB is the most devastating citrus disease worldwide and severely impacts the US citrus industry with millionaire losses annually due to the lack of an effective management approach (1). In this study, the in vitro antimicrobial activity of a Zinkicide™, a ZnO based nano-formulation, was evaluated in batch cultures and under flow conditions, using *Liberibacter crescens* (Lcr) as a biological model for *Liberibacter* spp. Zinkicide minimum inhibitory concentration in microtiter assays was 52ppm, while no colonies were recovered in BM7 agar plates from Lcr cultures treated with Zinkicide™ concentrations above 183ppm. The application of 104ppm of the compound inhibited more than the 96% of Lcr planktonic and biofilm fraction growth. Zinkicide™ was not effective against Lcr preformed biofilm in batch cultures in the minimum bactericidal concentration range. In microfluidic chambers (MC), Zinkicide™ did not remove Lcr cells adhered to the surface nor disrupted preformed biofilms, but the use of the LIVE/DEAD BactLight® cell viability kit inside these devices, revealed the occurrence of massive cell membrane damage in single cells and biofilms present on the Zinkicide™ treated channels. The spatial antimicrobial activity assessment of Zinkicide™ in MC also showed the influence of the cell numbers, structural channel splits and flow direction, on the antimicrobial activity of Zinkicide™ in a system mimicking '*Candidatus* Liberibacter asiaticus' (CLas) natural environment. The exposure of Lcr to different doses of the antimicrobial compound for two hours, showed that Lcr ROS production is positively correlated with Zinkicide™ concentration. These results demonstrate that Zinkicide™ is a suitable candidate for chemical control of CLas if it can reach phloem system as predicted for this nanoparticle.

Introduction

Citrus greening or Huanglonbing (HLB) is one of the most relevant plant disease for citrus-producing areas worldwide (2). The disease is associated with three different species that include '*Candidatus* Liberibacter asiaticus' (CLas) and '*C.* L. americanus'(CLam), which are vectored by the Asian citrus psyllid (ACP) *Diaphorina citri*, and a third species, '*Ca.* L. africanus'(CLaf), transmitted by the African citrus psyllid *Trioza erytreae* (3). In the US, HLB is caused by CLas and transmitted by ACP, and compromised the citrus industry with annual losses of more than 300 million dollars and the collateral elimination of thousands of citrus trees and more than 8,000 jobs lost (4).

The control of this disease is especially difficult due to the high dependence of its causal agents on both their vector insect and plant hosts (5). These pathogens are spread by highly mobile vector insects which difficult its contention in the initial infection focus and rapidly expand it to new areas (2). Inside their vector insect, these pathogens undergo a circulative transmission, reaching their major multiplication levels in the sheltered niche of the insect hemolymph (6, 7). Then, these bacterial pathogens are re-inoculated during the insect feeding from the insect salivary glands to another secluded intracellular environment, the plant phloem (8).

The phloem-limited habitat of these pathogens in their plant hosts makes conventional chemical control methods to fail or being economically inviable (2). Copper-based compounds have shown low efficacy at regular concentrations and are phytotoxic at effective concentrations (9). The injection of antibiotics such as oxytetracycline and penicillin has also been explored with relative effectiveness (10, 11), but this method has

been time consuming and expensive; applications need of trained personal to perform the activity, and requires trunk injections to deliver these antimicrobials in the plant phloem. The selective pressure applied to the microbial communities by the continued release of antibiotics in the environment also increases the risk of apparition of microbial resistance in animal, plant and human pathogens (5), limiting the use of this control method. Evolving in this close dependence with their hosts, has possibly caused pathogenic *Liberibacter* spp. to lose several genes required for free living behavior, resulting in very particular nutritional and environmental requirements that have not been elucidated yet, therefore precluding its growth in pure culture in vitro (12). The only culturable species of the genus is *Liberibacter crescens* (Lcr) (13). Despite the fact that no pathogenicity in any host has been proved for this member of the genus, Lcr displays more than the 77% of average nucleotide identity (ANI) with pathogenic *Liberibacter* spp. (14), and is described as a phloem inhabitant bacteria (13). These characteristics make of Lcr the best biological model to study the *Liberibacter* genus in vitro.

In the last couple of decades, nanoparticles have been extensively studied and have found practical applications in a variety of areas that include chemistry, engineering, physics, biology, and medicine (15). In drug delivery systems, the use of nanomaterials have brought a wide spectrum of forms with improved physicochemical characteristics and curative properties (16). Among them, zinc oxide (ZnO) nanoparticles represent an important class of commercially-available material and has been widely applied in diagnostics, therapeutics, drug-delivery systems, and food additives, among other fields, due to their magnetic, catalytic, semiconducting, antimicrobial, and binding properties (17).

Zinkicide™, is a novel nano-formulated zinc oxide compound designed with the goal to control bacterial citrus diseases. This compound showed a two-fold lower minimum inhibitory concentration in vitro (MIC) against *Xanthomonas citri* subsp. *citri*, *Escherichia coli* and *X. alfalfae* subsp. *citrumelonis* than copper-based compounds (9). When applied to citrus plants in the field, Zinkicide™, was more effective at reducing incidence of citrus canker than traditional copper-based compounds (9).

The potential of this compound to control pathogenic *Liberibacter* spp. relies on its small particle size, that allows this compound to ionize faster increasing its antimicrobial properties and its metallic zinc based nature (an essential nutrient for the plant), that improves overall plant performance and reduces phytotoxicity (18). All these features point at Zinkicide™ as a promising chemical control of diseases caused by pathogenic *Liberibacter* spp. In this work we evaluated the antimicrobial effect and studied the mode of action of Zinkicide™ in vitro, using *Liberibacter crescens* type strain BT-1 (Lcr) as a biological model for the *Liberibacter* genus. As main findings, we observed that Zinkicide™ effectively inhibit growth and biofilm formation of this bacterium, while it was not effective against Lcr preformed biofilms. These features make this compound feasible for chemical control of HLB, but its impact on CLas biology and insect transmission require of further testing under field conditions.

Materials and Methods

Bacterial strains and culture conditions

Liberibacter crescens strain BT-1 (13) was used in this study. BT-1 Lcr strains were grown on BM7 agar solid medium at 28°C. Stocks of Lcr cultures were stored in BM7 broth plus 20% glycerol at -80°C. Lcr cultures in BM7 broth were used for minimum inhibitory concentration (MIC) and minimum bactericidal concentration assays (MBC). For biofilm formation inhibition and microfluidic chambers assays, Lcr strains where initially grown from glycerol stocks in BM7 agar plates and then the mBM7 medium, the formulation previously optimized in Chapter 1 for Lcr biofilm formation.

MIC and MBC determination

Zinkicide™ MIC and MBC assays were performed in polystyrene 96 well plates (COSTAR®, Kennebunk, ME. USA). Wells placed at the edges of the 96 well plates were initially filled with 250µl of sterile deionized water to avoid desiccation. Then, 10µl of Lcr bacterial suspension in BM7 (OD_{600}=1, for a final OD_{600}=0.07), were inoculated onto 190µl of BM7 supplemented with a Zinkicide™ concentration gradient from 0 to 104ppm for MIC determination and from 131 to 209ppm for MBC. Six blank wells and six well treatment replicates were included for each treatment. Plates were wrapped with parafilm and incubated at 28°C, 150rpm for 7 days. At the end of the incubation time, the absorbance at 600nm of each treatment and blank was read using a Cytation 3 Image Reader spectrophotometer (BioTek Instruments Inc, Winooski, Vermont, USA). Total

growth was calculated by subtracting each blank absorbance value from the inoculated culture turbidity. Significant differences among treatments OD_{600}, were determined using ANOVA and Fisher Least Significant Difference (LSD) method, at a significance level of $P < 0.05$ using the SIGMA Plot Software (Version 11.0). MIC was determined as the lower Zinkicide™ treatment were no increase in initial culture turbidity ($OD_{600} \leq 0.07$) was observed. For MBC, 100µl of three well replicates for each concentration from 131 to 235ppm were dropped in BM7 agar plates, extended with sterile cell spreaders and incubated in a moisture chamber at 28°C for one month. The MBC was determined as the treatment were no colonies were recovered in BM7 agar plates after one month of incubation period. The experiments were repeated two times independently.

Biofilm formation inhibition and biofilm disruption assays in batch cultures

For biofilm formation inhibition and biofilm disruption assays, mBM7 was used for Lcr bacterial suspension preparation and biofilm formation in 96 well plates. For biofilm inhibition assays, treatments were inoculated and incubated as described above for MIC determination. Total and planktonic growth were determined by OD_{600} readings at 8dpi while biofilm formation inhibition was assessed using the crystal violet biofilm staining protocol (19). For biofilm disruption assays, Lcr cultures were inoculated as described above in mBM7, and allowed to form biofilm for 7 days. At this time, entire culture volumes were aseptically removed, including blanks and Lcr inoculated wells, and were resuspended in 200µl of mBM7 and a Zinkicide™ concentration gradient in the range used for the MBC (131-209ppm). Resuspended cultures were incubated for 8 additional days under the same conditions. Then, Lcr cultures were assessed for total, planktonic and

biofilm formation as described above. Blank absorbance values were subtracted from biofilm growth values for each treatment. Significant differences in turbidity readings between the total and the biofilm growth for each treatment were calculated by ANOVA and Fisher Least Significant Difference (LSD) method. Significant differences between the planktonic growth for each treatment was determined using a Kruskal-Wallis One Way Analysis of Variance on Ranks. All the statistical analyses were performed at the significance level $P < 0.05$, using SIGMA Plot Software (Version 11.0).

Biofilm formation inhibition and biofilm disruption assays in microfluidic chambers

Microfluidic chamber design and fabrication was performed as previously described (20). For biofilm formation inhibition assays the upper channel was initially filled with mBM7 in the lower channel and mBM7 supplemented with Zinkicide™ 78ppm using an automated syringe pump (Pico Plus; Harvard Apparatus, Holliston, MA). Lcr bacterial suspensions in mBM7 (OD_{600nm}=0.5) were injected for one hour to obtain attached cells. After a critical number of attached cells was observed (~ 5 cells/20μm^2), bacterial cultures inlets were clamped with surgical scissors, and the flow rate was maintained constant at 0.25µl/min for 7 days. For biofilm disruption assays, both channels were initially filled with mBM7 and Lcr cells were inoculated as described above and allowed to form biofilm for 10 days. After this time, the culture media in one of the channels was replaced by mBM7 supplemented with 131ppm of Zinkicide™ and allowed to flow at the same rate for 10 additional days. MC were mounted onto a Nikon Eclipse Ti inverted microscope (Nikon, Melville, NY) and observed with a 40X objective using phase contrast and Nomarski differential interference contrast (DIC) optics. Cell division over time was

recorded using time-lapse video imaging microscopy. Image acquisition was performed automatically every 10min using a Nikon DS-Q1 digital camera (Nikon, Melville, NY) controlled by NIS- Elements software version 3.0 (Nikon, Melville, NY). At the end time point of the experiments Lcr cell viability inside the MC was assessed using the LIVE/DEAD® BactLight Bacterial viability kit. Briefly, 3µl of each reagent of the kit was added to 1ml of the same treatments running in the MC, loaded into a 1ml plastic syringe (BD Becton Dickinson, Utah, USA), aseptically interchanged by the treatment running in the MC, and inoculated under the dark at the same flow rate used above. To detect both dyes used, propidium iodide and SYTO 9, excitation wavelengths of 528 (FITC) and 590 (TRTC), respectively, were used. Image capture and analysis was performed using a Nikon Eclipse Ti inverted microscope (Nikon, Melville, NY) fitted with a Nikon DS-Q1 digital camera (Nikon, Melville, NY) controlled by NIS- Elements software version 3.0 (Nikon, Melville, NY). At least two independent experiments were performed.

Reactive oxygen species (ROS) formation quantification

L. crescens ROS production in response to Zinkicide™ was determined using the general oxidative stress indicator CM-H_2DCFDA (ThermoFisher Scientific). Briefly, 6 days-old Lcr cells in BM7 agar plates were scrapped and suspended in pre-warmed (28°C) phosphate buffer saline (PBS) (OD_{600}= 1) with a 5µM dye concentration and incubated for 15 min at 28°C at 150rpm. Then, Lcr cells were centrifuged at 4,000rpm for 5min, the excess of dye was removed with the buffer and the cells were resuspended and homogenized in fresh PBS. Then 10µl of the resuspended cells where inoculated in a Zinkicide™ concentration gradient form 0 to 78ppm. To quantify the effect of

Zinkicide™ in the emission intensity of the dye in absence of cells, additional treatments of the same Zinkicide™ concentrations, where inoculated with the dye at a final concentration of 0.5µM. Three replicates were tested for each cell free and cell inoculated treatment. Fluorescence intensity was read with excitation/emission wavelengths of 492 and 517 nm, respectively, using a using a Cytation 3 Image Reader spectrophotometer (BioTek Instruments Inc, Winooski, Vermont, USA). To normalize the data as a function the dye emission for each Zinkicide™ concentration value, the emission with the cell free-Zinkicide™ free treatment (BM7 plus 0.5µM of CM-H_2DCFDA), was divided by the emission obtained for each cell free treatment, including itself, and these values were saved as the signal inhibition factor for each treatment. Then, each signal inhibition factor, was multiplied by the emission of its corresponding cell inoculated replicates and were averaged to obtain the final ROS production values for each cell inoculated treatment. Significant differences among treatments ROS production, were determined using ANOVA and Fisher Least Significant Difference (LSD) method, at a significance level of $P < 0.05$ using SIGMA Plot Software (Version 11.0).

Results

MIC and MBC determination assays

Zinkicide™ significantly inhibited Lcr growth for all the concentration tested (Fig 3-1). No significant increase in Lcr total growth and close average turbidity values were observed for Zinkicide™ concentrations from 52 (MIC) to 104ppm. In this range, Zinkicide™ inhibited the 85.6% of Lcr growth (as assessed by turbidity at 600nm). The MBC assay showed Zinkicide™ totally suppressed Lcr growth in BM7 agar plates at

concentration values above 183ppm. An average of 170 CFU/ml was recovered from the 157ppm Zinkicide™ treatment and more than 300 colonies were recovered from lower concentrations (Table 3-1).

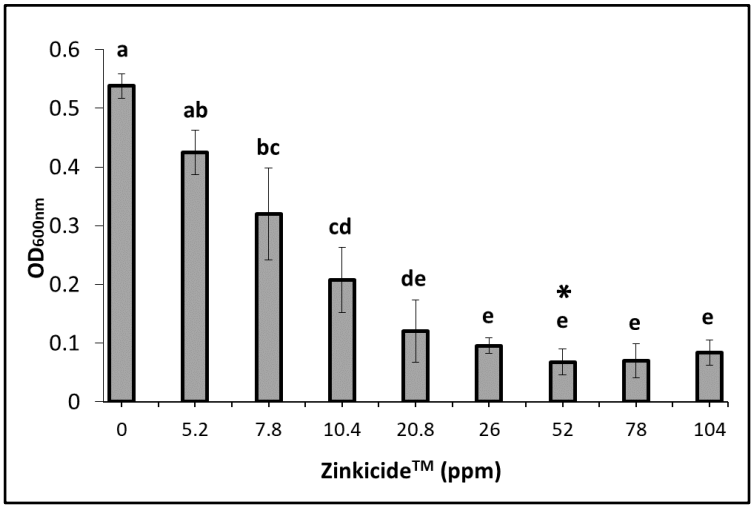

FIGURE 3-1. Lcr total growth inhibition from 0 to 104ppm of Zinkicide™ in BM7 medium. Lcr culture OD_{600} are represent as mean values ± standard deviations (SD) in single bars for each treatment (n=6). Different letters represent significant differences calculated by a Fisher-LSD method at the significant level of $P < 0.05$. * Minimum inhibitory concentration.

Table 3-1. Colony forming units per ml (CFU/ml) recovered in BM7 agar plates for each Zinkicide™ concentration value tested in the MBC concentration range.

Zinkicide™ (ppm)	**131**	**157**	**183**	**209**
CFU/ml in BM7	>300	170±39	0	0

Biofilm formation inhibition and biofilm disruption activity of Zinkicide™

The planktonic culture fraction showed no significant differences in growth inhibition for all the Zinkicide™ concentrations tested in this assay with inhibition percentages above 96%. The biofilm growth fraction showed no significant differences between the Zinkicide™ treated samples but progressively inhibited Lcr biofilm formation from 71.5 to 96.1%. Finally, the total growth displayed a balance between these two previous culture fractions, with inhibition values from 86.7 to 94.2% (Fig 3-2).

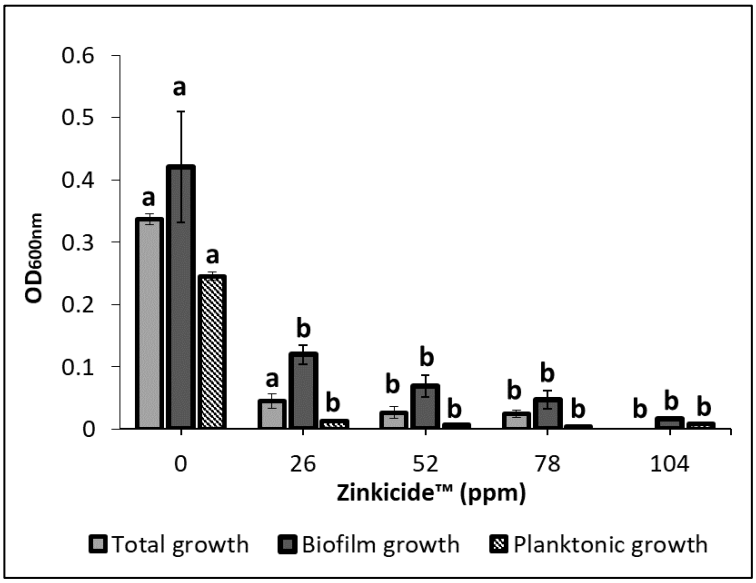

Figure 3-2. Biofilm formation inhibition activity of Zinkicide™ against Lcr. Total, planktonic and biofilm growth for the untreated cultures (0ppm) and the Zinkicide™-treated cultures are represented as mean values ± SD in three different bars for each treatment (n=6). Different letters for the total and the biofilm growth represent significant differences calculated by a Fisher-LSD method. Different letters for the planktonic growth represent significant differences determined by a Kruskal-Wallis One Way Analysis of Variance on Ranks. All statistical analyses were performed at a significance level of $P <$

0.05. Two independent experiment were performed, and one representative experiment is shown.

Zinkicide™ did not disrupt Lcr preformed biofilms. No significant differences were observed between the untreated control and the treatments from 131 to 183ppm, while the biofilm formation was significantly higher in the 209ppm Zinkicide™ treatment (Fig 3-3).

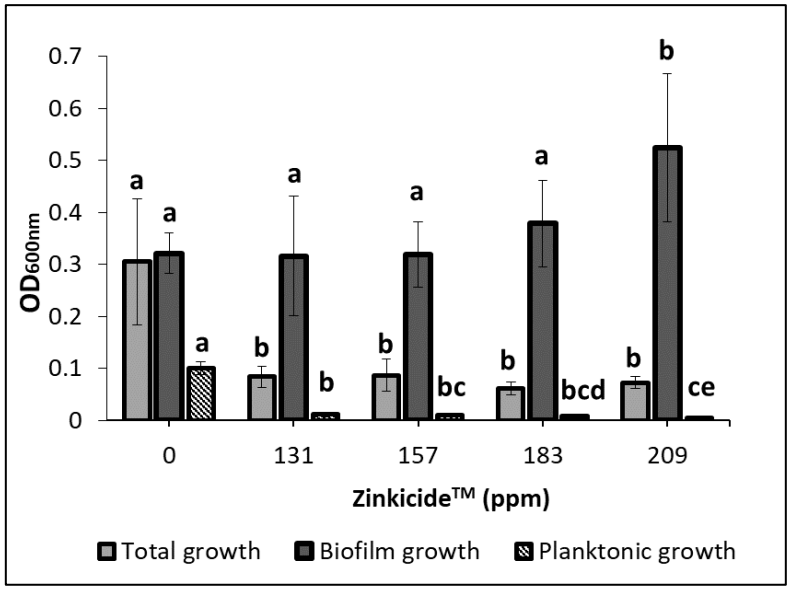

Figure 3-3. Zinkicide™ effect on Lcr preformed biofilms 8 days after application. Total, planktonic and biofilm growth for the untreated cultures (0ppm), and the Zinkicide™ treated cultures are represented as mean values ± SD in three different bars for each treatment (n=6). Different letters for the total and the biofilm growth, represent significant differences calculated by Fisher-LSD method. Different letters for the planktonic fraction represent significant differences determined by a Kruskal-Wallis One Way Analysis of Variance on Ranks. All statistical analyses were performed at a

significance level of $P < 0.05$. Two independent experiments were performed, and one representative experiment is shown.

Biofilm formation inhibition and disruption by Zinkicide™ in microfluidic chambers

Time-lapse images in MC captured during biofilm formation assays showed Lcr stopped cell division in the Zinkicide™-treated channel, meanwhile an active cell division that resulted in a final increased biofilm formation was observed in the untreated control channel. No evidence of cell detachment was observed during this experiment in the Zinkicide™-treated channel (Fig 4-A, left panel). The use of the LIVE/DEAD® BactLight Bacterial viability kit, revealed that the remaining attached cells in the Zinkicide™ treated channel had compromised cell membranes because of their staining with the cell impermeable DNA intercalant agent propidium iodine (Fig 4-A, right panel). The biofilm disruption assay showed Zinkicide™ did not cause a significant qualitative biofilm disruption in Lcr preformed biofilms during the time tested (Fig 4-B, left panel), however, the LIVE/DEAD® BactLight Bacterial viability kit also revealed the occurrence of massive membrane damage and very few viable cells in the remaining attached biofilm (Fig 4-B, right panel).

A more general view of the spatial antibacterial activity of Zinkicide™ against Lcr in MC was obtained by merging the images obtained from different sections of the MC device after staining with the LIVE/DEAD® BactLight Bacterial viability kit. As shown in the Fig 5, there is a gradient in the proportion of dead and live cells, with a decrease in the number of dead cells in areas farther from the main channel where the Zinkicide™ was

applied, and a decrease in live cells in areas farther from the lateral inlet used for bacterial inoculation (Fig 5).

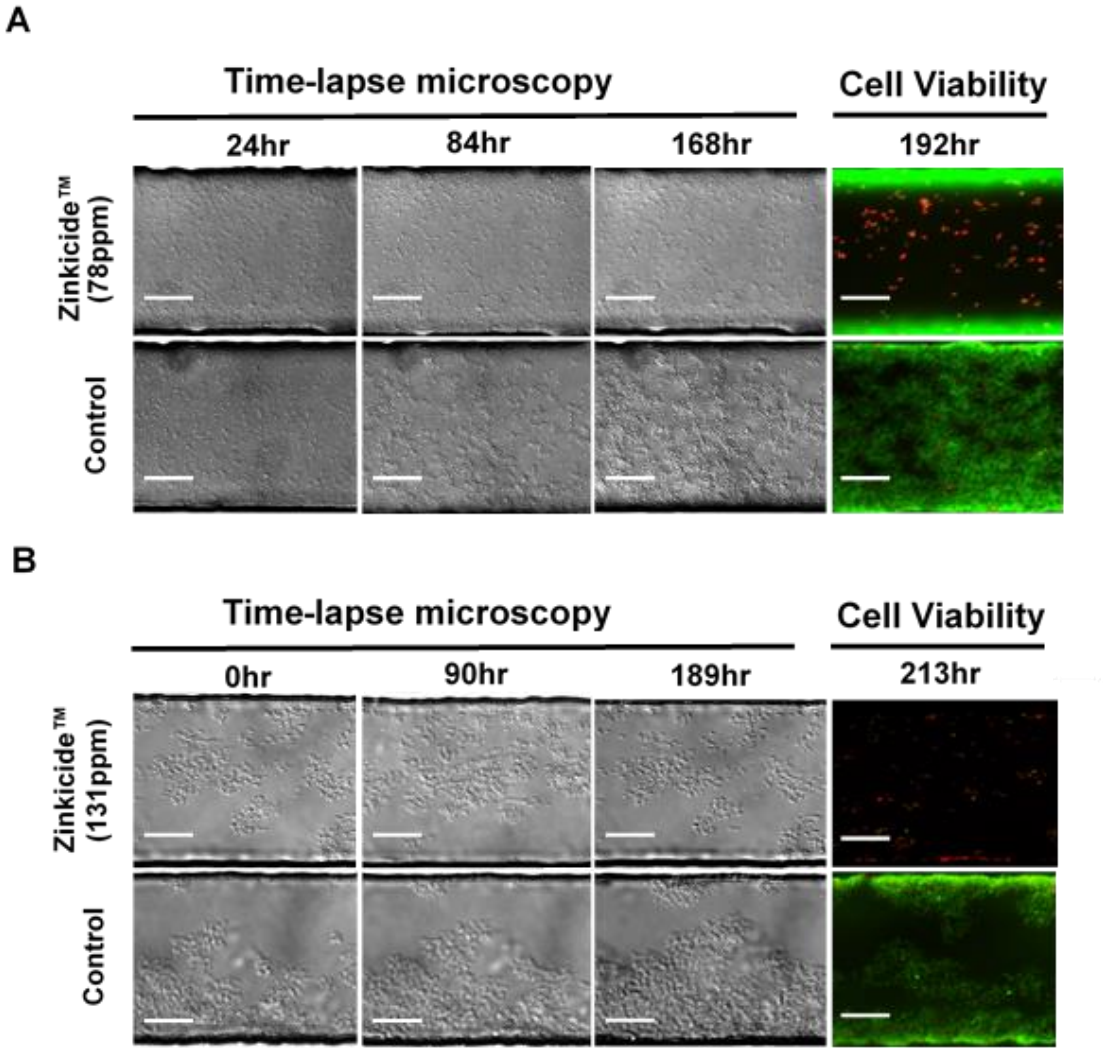

Figure 3-4. Biofilm formation inhibition and biofilm disruption assays in microfluidic chambers. A) Biofilm formation inhibition assay. B) Biofilm disruption assay. Left panel: Time-lapse (DIC) microscopy. Right panel: cell viability assessing with the LIVE/DEAD® BactLight Bacterial viability kit. Scale bar: 20µm.

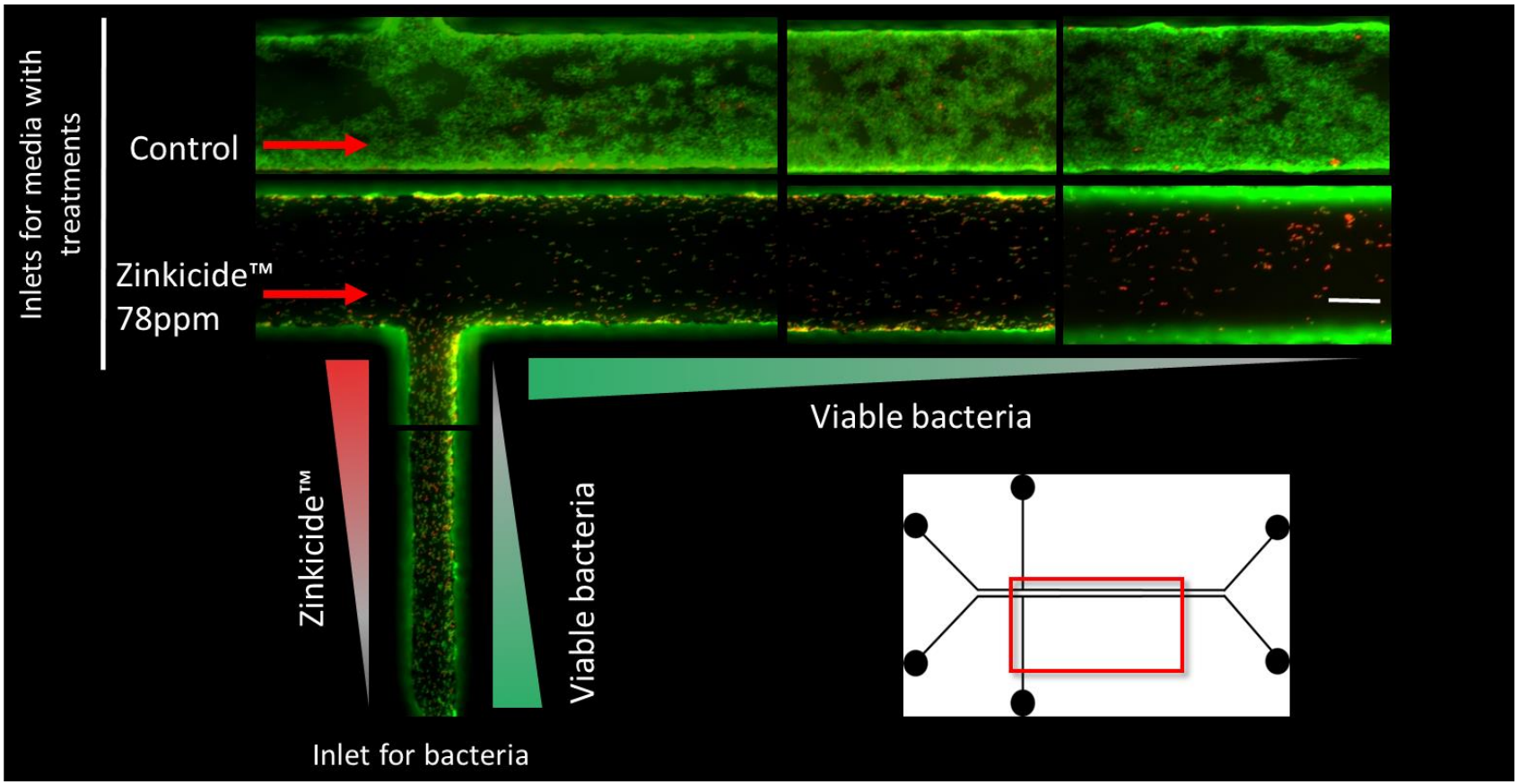

Figure 3-5. Spatial antibacterial activity of Zinkicide™, against Lcr in microfluidic chambers (MC) assessed by the LIVE/DEAD® BactLight Bacterial viability kit. The red section marked in the diagram in white background shows the area of the MC represented in the image. Scale bar: 20µm.

Lcr ROS production in response to Zinkicide™

As was expected from its chemical properties, Zinkicide™ interfered in a dose manner with the general oxidative stress indicator CM-H_2DCFDA fluorescence emission (Fig 6-A). As result of this interference, no clear trend in Lcr ROS production was observed in the Zinkicide™ cell inoculated treatments, in comparison with the untreated control replicates (Fig 6-C). After fluorescence emission normalization, an increase in ROS formation was observed in response to Zinkicide™ concentration increase (Fig 5-C). A linear regression analysis showed Lcr ROS production was positively correlated with Zinkicide™ concentration in the tested range (Fig 6-D).

Discussion

Zinkicide™ has a lower MIC compared with ZnO based nanoparticles tested in other studies and therefore a more potent antimicrobial activity. The MIC for Zinkicide™ against Lcr determined in this study was as low 52ppm. This value is approximately more than five-fold lower than MIC values determined for different metal nanoparticles, comprising ZnO, CuO and $AgTiO_2$, against several human and fish pathogens such as *Staphylococcus aureus, Pseudomonas aeruginosa, Vibrio* spp. and *Flavobacterium, Branchiophylum* and fungus of the genus *Penicillium* and *Mucor* (21). Lower MIC values have been reached in other studies were Catechin-Cu nanoparticles had MIC values of 20 and 10ppm for *Echerichia coli* and *S. aureus*, respectively (22) and another report were silver nanoparticles were tested against *S. aureus*, *E. coli*, *Bacillus cereus* and *Pseudomonas putida*, showing MIC values above 2-4ppm (23).

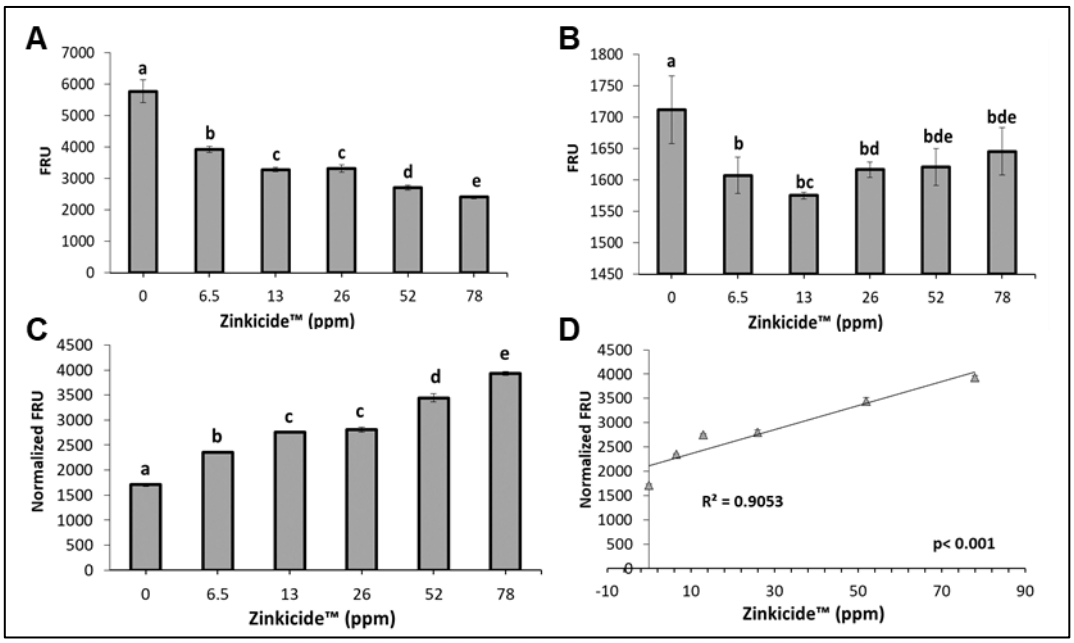

Figure 3-6. *L. crescens* ROS formation in response to Zinkicide™. A) CM-H_2DCFDA fluorescence relative units (FRU) emission in each Zinkicide™ treatment in cell free assays. B) Total FRU values obtained for cell inoculated assays. C) Normalized FRU values for cell inoculated treatments. Different letters represent significant differences determined by Fisher-LSD method at the significance level of $P < 0.05$. Error bars: standard deviations. D) Lineal regression between the normalized FRU for the cell inoculated treatments and Zinkicide™ concentration.

Zinkicide™ concentration value of 104ppm inhibited more than the 96% Lcr biofilm formation. However, as was expected, the biofilm fraction showed a lower sensitivity to Zinkicide™ than the planktonic phase. Biofilms are well known as persistent multicellular structures wherein several microbial resistance mechanisms can occur (24, 25). Insufficient antimicrobial compound diffusion can be reached inside the biofilm due to the mechanical and physicochemical properties of the biofilm matrix leading to bacterial

survival due to the low dose of antimicrobial inside the biofilm (26). Antimicrobial compounds can also be inactivated by chemical reaction with the extracellular components of the biofilm or by attaching to the anionic polysaccharides without reaching to the target bacterial cells (27). The differential distribution of nutrients and oxygen inside the biofilm also cause a heterogeneity in growth rate and metabolism, and makes less active cells more resilient to antimicrobial compounds (10). In this regard, Zinkicide™ was ineffective against Lcr preformed biofilms and caused a numerical increase of biofilm formation by Lcr. These results are in consistence with previous studies in *Xylella fastidiosa* that showed that the exposition of this pathogen to high doses of the metallic compound, reduced the pathogen cultivability but increased the exopolysaccharides production and biofilm formation as a resistance mechanism, likely induced by the stress response of Zinkicide™ exposure (28). Wu et al. described similar results when testing the biofilm disruption activity of Zn against bacterial swine pathogens (29). It has been described that positively charged molecules, such as Zn ions, are prone to be captured by the overall negative charge of biofilm extracellular matrix, conferred by their EPS chemical groups (30). For *X. fastidiosa*, it was theorized that Zn ions accumulate the extracellular matrix, delaying Zn ions penetration to the sessile cells, and consequently, reducing Zn intracellular levels and toxicity (28).

MC assays showed the effect of Zinkicide™ against Lcr biofilms under flow conditions that more closely resemble the natural environment of *Liberibacter* spp. Zinkicide™ did not reduce Lcr attachment to surfaces in any of the assays performed in MC. Considering knowledge in other nanoparticles, it is expected that Zinkicide™ affects protein activity by direct binding and inactivation, or by the collateral protein damage caused by the increase in intracellular ROS (31, 32). However, and how we described in Chapter 1,

protein synthesis disruption does not impact on Lcr cell-surface attachment, therefore may be expected Zinkicide™ does not detach Lcr cell from the surfaces.

On the other hand, Zinkicide™ was able to cause death to Lcr cells adhered to surfaces inside MC and 10-days old preformed biofilms in the MC, showing its penetration capacity inside Lcr biofilms. Improvements in nanoparticle size and shape have been carried out in order to enhance the penetration of these compounds into bacterial biofilms (27).

The use of the LIVE/DEAD® BactLight Bacterial viability kit to assess Lcr viability inside MC also helped to understand the distribution of Zinkicide™ in an interconnected tubular niche with different flow rates, Zinkicide™ concentrations and cell densities. Since the lateral inlets are clamped and Zinkicide™ treatments flow through the main channel, just sub-inhibitory concentrations of the compound penetrate the lateral inlets and a concentration gradient of the antimicrobial compound is formed from the main channel to the end of the inlet for bacteria (Fig 5). At the same time, the lateral inlets for bacteria are more highly occupied by bacteria because they receive the initial bacterial inoculum at a high cell density. As result, a decrease in Lcr cell viability is observed from the end of the lateral inlet for bacteria, where more viable attached cells and/or biofilms are observed, to the connection with the main channel where the Zinkicide™ is mostly flowing at inhibitory concentrations. It has been described an increase in *E. coli* viability when these are treated with ZnO nanoparticles at sub-inhibitory concentration (33). Previous works also demonstrated cell density also influences the antimicrobial activity of ZnO nanoparticles with a negative correlation between the bacterial density and the antimicrobial activity of the compound (34, 35). These results have relevance to

understand the spatial distribution of the Zinkicide™ in relation with the initial application point and the influence of cell density on its antibacterial activity.

Zinkicide™ significantly interfered with CM-H_2DCFDA fluorescence emission when added to cell free treatments. This process is called photobleaching and results from the conversion of fluorescent dye molecules into fluorophores that are unable to fluoresce (36). As result of this process the Zinkicide™ cell inoculated treatments displayed a lower emission than the untreated cell inoculated samples. Zinkicide™ formulation contains hydrogen peroxide, which is known it can directly bind and destroy the fluorescent dyes (37). Therefore, we attributed the effect we observed in the cell free treatments to a reduction of the fluorescence emission caused by this interaction. Since the fluorescence emission of our cell inoculated treatments was biased by this process, we first quantified the influence of Zinkicide™ formulation in the dye emission as factors, and later we used these factors to normalize the data obtained from the cell inoculated treatments.

After data normalization, Lcr exposure to increasing Zinkicide™ concentrations resulted in an increase on ROS production in a dose-dependent manner. ROS formation has been described as the main mode of action of metal nanoparticles (31, 38, 39). In contact with water in solution, ZnO nanoparticles trigger a series of chemical reactions that produces peroxide, superoxide and hydrogen peroxide species (40, 41). The two first reactive species are cell impermeable and remain attached to the membrane, but the hydrogen peroxide penetrates and acts intracellularly (42). The consequent change on the oxidative status inside the cell and of the surroundings, causes severe cell structural and functional injury that includes cell wall damage due to ZnO-localized interaction, internalization of nanoparticles due to loss of proton motive force, increased membrane permeability and

intake of toxic dissolved zinc ions, among others effects that eventually lead to cell death (31).

The reduced genome of CLas in comparison with Lcr (14) and the lack of free living genes of this pathogen, especially those to cope with oxidative stress (12), suggest a similar or higher antimicrobial activity can be achieved by Zinkicide™ against CLas. However, factors such as CLas intracellular nature, its irregular distribution on the plants and the unknown plant detoxification mechanisms influence in Zinkicide™ concentrations, can modulate this activity, therefore, they need to be fully addressed in order to obtain better results with Zinkicide™ as a chemical control agent. In this sense, the observed influence of Zinkicide™ on Lcr preformed biofilms may serve as a warning about the collateral impact that the application of this compound may have in CLas biofilms formed in the insect digestive system. Field trials testing the efficacy of Zinkicide™ against CLas on infected citrus plants and studies to assess the distribution and persistence of the compound in the treated plants are being carried on currently (43). Factors such as application method, time between product applications and the evaluation of the environmental impact resulting of its use, are the next steps to make of Zinkicide™ and effective and safe therapeutic method to reduce CLas populations in the critical situation of Florida. At the same time, and no less important, this work should be complemented by assessing the influence of the application of this compound on CLas populations in the insect vector, as inseparable part of CLas life cycle. The combined application of this and other management methods, as part of an integrated disease management, will help to reduce the economic and collateral impact of this devastating citrus disease.

References

1. Committee on a Review of the Citrus Greening Research and Development Efforts. 2018. A Review of the Citrus Greening Research and Development Efforts Supported by the Citrus Research and Development Foundation: Fighting a Ravaging Disease. Natl Acad Press.

2. Wang N, Pierson EA, Setubal JC, Xu J, Levy JG, Zhang Y, Li J, Rangel LT, Martins J. 2017. The *Candidatus* Liberibacter–Host Interface: Insights into Pathogenesis Mechanisms and Disease Control. Annu Rev Phytopathol 55:451–482.

3. Wang N, Trivedi P. 2013. Citrus Huanglongbing: A Newly Relevant Disease Presents Unprecedented Challenges. Phytopathology 103:652–665.

4. Hodges AW, Spreen TH. 2012. Economic impacts of citrus greening (HLB) in Florida, 2006/07-2010/11. EDIS FE903:1–6.

5. Blaustein RA, Lorca GL, teplitski max. 2017. Challenges for Managing *Candidatus* Liberibacter spp. (Huanglongbing disease pathogen): Current Control Measures and Future Directions. Phytopathology PHYTO-07-17-0260-RVW.

6. Ghanim M, Fattah-Hosseini S, Levy A, Cilia M. 2016. Morphological abnormalities and cell death in the Asian citrus psyllid (Diaphorina citri) midgut associated with Candidatus Liberibacter asiaticus. Sci Rep 6:1–11.

7. Canale MC, Tomaseto AF, Haddad M de L, Della Coletta-Filho H, Lopes JRS. 2017. Latency and Persistence of " *Candidatus* Liberibacter asiaticus" in Its Psyllid Vector, *Diaphorina citri* (Hemiptera: Liviidae). Phytopathology 107:264–272.

8. Vyas M, He R, Nelson W, Yin G, Cicero JM, Willer M, Kim R. 2018. Asian Citrus Psyllid Expression Profiles Suggest "Candidatus Liberibacter asiaticus"-Mediated Alteration of Adult Nutrition nd Metabolism, and of Nymphal Development and Immunity. PLoS One 10:1–20.

9. Graham JH, Johnson EG, Myers ME, Young M, Rajasekaran P, Das S, Santra S.

2016. Potential of Nano-Formulated Zinc Oxide for Control of Citrus Canker on Grapefruit Trees. Plant Dis 100:2442–2447.

10. Zhang M, Guo Y, Powell CA, Doud MS, Yang C, Duan Y. 2018. Effective Antibiotics against " Candidatus Liberibacter asiaticus " in H ... Effective Antibiotics against " Candidatus Liberibacter asiaticus " in H ... 1–10.

11. Zhang M, Yang C, Powell CA. 2015. Application of antibiotics for control of citrus huanglongbing. Adv Antibiot Antibodies 1:e101.

12. Lai KK, Davis-Richardson AG, Dias R, Triplett EW. 2016. Identification of the genes required for the culture of Liberibacter crescens, the closest cultured relative of the Liberibacter plant pathogens. Front Microbiol 7:1–11.

13. Leonard MT, Fagen JR, Davis-Richardson AG, Davis MJ, Triplett EW. 2012. Complete genome sequence of Liberibacter crescens BT-1. Stand Genomic Sci 7:271–283.

14. Wang J, Haapalainen M, Schott T, Thompson SM, Smith GR, Nissinen AI, Pirhonen M. 2017. Genomic sequence of "Candidatus Liberibacter solanacearum" haplotype C and its comparison with haplotype A and B genomes. PLoS One 12:1–21.

15. Zaman M, Ahmad E, Qadeer A, Rabbani G, Khan RH. 2014. Nanoparticles in relation to peptide and protein aggregation. Int J Nanomedicine 9:899–912.

16. Dizaj SM, Lotfipour F, Barzegar-Jalali M, Zarrintan MH, Adibkia K. 2014. Antimicrobial activity of the metals and metal oxide nanoparticles. Mater Sci Eng C 44:278–284.

17. Choi SJ, Choy JH. 2014. Biokinetics of zinc oxide nanoparticles: Toxicokinetics, biological fates, and protein interaction. Int J Nanomedicine 9:261–269.

18. Farooq M, Wahid A, Kobayashi N, Fujita D, Basra SM a. 2009. Sustainable AgricultureSustainable Agriculture.

19. Zaini PA, De La Fuente L, Hoch HC, Burr TJ. 2009. Grapevine xylem sap enhances biofilm development by Xylella fastidiosa. FEMS Microbiol Lett 295:129–134.

20. De La Fuente L, Montanes E, Meng Y, Li Y, Burr TJ, Hoch HC, Wu M. 2007. Assessing adhesion forces of type I and type IV pili of Xylella fastidiosa bacteria by use of a microfluidic flow chamber. Appl Environ Microbiol 73:2690–2696.

21. Swain P, Nayak SK, Sasmal A, Behera T, Barik SK, Swain SK, Mishra SS, Sen AK, Das JK, Jayasankar P. 2014. Antimicrobial activity of metal based nanoparticles against microbes associated with diseases in aquaculture. World J Microbiol Biotechnol 30:2491–2502.

22. Li H, Chen Q, Zhao J, Urmila K. 2015. Enhancing the antimicrobial activity of natural extraction using the synthetic ultrasmall metal nanoparticles. Sci Rep 5:1–13.

23. Jain N, Bhargava A, Rathi M, Dilip RV, Panwar J. 2015. Removal of protein capping enhances the antibacterial efficiency of biosynthesized silver nanoparticles. PLoS One 10:1–19.

24. Singh S, Singh SK, Chowdhury I, Singh R. 2017. Understanding the Mechanism of Bacterial Biofilms Resistance to Antimicrobial Agents. Open Microbiol J 11:53–62.

25. Wei Q, Ma LZ. 2013. Biofilm matrix and its regulation in Pseudomonas aeruginosa. Int J Mol Sci 14:20983–21005.

26. Lebeaux D, Ghigo J-M, Beloin C. 2014. Biofilm-Related Infections: Bridging the Gap between Clinical Management and Fundamental Aspects of Recalcitrance toward Antibiotics. Microbiol Mol Biol Rev 78:510–543.

27. Kingdom U, Kingdom U, London F, Health N, Foundation S, Kingdom U, Kingdom U. 2017. HHS Public Access 21:129–139.

28. Navarrete F, De La Fuente L. 2014. Response of Xylella fastidiosa to zinc: Decreased culturability, increased exopolysaccharide production, and formation of resilient biofilms under flow conditions. Appl Environ Microbiol 80:1097–1107.

29. Wu C, Labrie J, Tremblay YDN, Haine D, Mourez M, Jacques M. 2013. Zinc as an agent for the prevention of biofilm formation by pathogenic bacteria. J Appl Microbiol 115:30–40.

30. Sutherland IW. 2001. Biofilm exopolysaccharides: A strong and sticky framework. Microbiology 147:3–9.

31. Sirelkhatim A, Mahmud S, Seeni A, Kaus NHM, Ann LC, Bakhori SKM, Hasan H, Mohamad D. 2015. Review on zinc oxide nanoparticles: Antibacterial activity and toxicity mechanism. Nano-Micro Lett 7:219–242.

32. Ramasamy M, Lee J. 2016. Recent nanotechnology approaches for prevention and treatment of biofilm-associated infections on medical devices. Biomed Res Int 2016.

33. Lee J, Kornfeld H. 2010. NIH Public Access. J Cell Death 36:490–499.

34. Yamamoto O. 2001. Influence of particle size on the antibacterial activity of zinc oxide. Int J Inorg Mater 3:643–646.

35. Nair S, Sasidharan A, Divya Rani V V., Menon D, Nair S, Manzoor K, Raina S. 2009. Role of size scale of ZnO nanoparticles and microparticles on toxicity toward bacteria and osteoblast cancer cells. J Mater Sci Mater Med 20:235–241.

36. Valeur B and MNB-S. 2012. Molecular Fluorescence. Principles and Applications. Second Edition 17–19.

37. Platkov M, Tirosh R, Kaufman M, Zurgil N, Deutsch M. 2014. Photobleaching of fluorescein as a probe for oxidative stress in single cells. J Photochem Photobiol B Biol 140:306–314.

38. Brayner R, Ferrari-Iliou R, Brivois N, Djediat S, Benedetti MF, Fiévet F. 2006. Toxicological impact studies based on Escherichia coli bacteria in ultrafine ZnO nanoparticles colloidal medium. Nano Lett 6:866–870.

39. Jan T, Iqbal J, Ismail M, Zakaullah M, Haider Naqvi S, Badshah N. 2013. Sn doping induced enhancement in the activity of ZnO nanostructures against antibiotic resistant S. aureus bacteria. Int J Nanomedicine 8:3679–3687.

40. Jin SE, Hwang W, Lee HJ, Jin HE. 2017. Dual UV irradiation-based metal oxide nanoparticles for enhanced antimicrobial activity in Escherichia coli and M13 bacteriophage. Int J Nanomedicine 12:8057–8070.

41. Padmavathy N, Vijayaraghavan R. 2008. Enhanced bioactivity of ZnO nanoparticles: An antimicrobial study. Sci Technol Adv Mater 9.

42. Zhang L, Jiang Y, Ding Y, Povey M, York D. 2007. Investigation into the antibacterial behaviour of suspensions of ZnO nanoparticles (ZnO nanofluids). J Nanoparticle Res 9:479–489.

43. Jhonson EG. 2015. ZINKICIDE A NANOTHERAPEUTIC FOR HLB. Res Educ Econ Inf Syst United States Dep Agric.